

# Vasculature Guides Migrating Neuronal Precursors in the Adult Mammalian Forebrain via Brain-Derived Neurotrophic Factor Signaling

Marina Snapyan,<sup>1\*</sup> Morgane Lemasson,<sup>1\*</sup> Monika S. Brill,<sup>3,4</sup> Mathieu Blais,<sup>5</sup> Mireille Massouh,<sup>1,2</sup> Jovica Ninkovic,<sup>3,4</sup> Claude Gravel,<sup>2,6</sup> François Berthod,<sup>5</sup> Magdalena Götz,<sup>3,4</sup> Philip A. Barker,<sup>7</sup> André Parent,<sup>2</sup> and Armen Saghatelyan<sup>1,6</sup>

<sup>1</sup>The Cellular Neurobiology Unit and <sup>2</sup>The Systemic Neurobiology Unit, Centre de Recherche Université Laval Robert-Giffard, Québec, Québec, Canada G1J 2G3, <sup>3</sup>Department of Physiological Genomics, Institute of Physiology and Center for Integrated Protein Science Munich, Ludwig Maximilian University Munich, D-80336 Munich, Germany, <sup>4</sup>Institute for Stem Cell Research, Helmholtz Zentrum München–National Research Center for Environmental Health, D-85764 Neuherberg/Munich, Germany, <sup>5</sup>Laboratoire d'Organogénèse Expérimentale, Centre Hospitalier Affilié Universitaire de Québec, Département de Chirurgie, Université Laval, Hôpital du Saint-Sacrement, Québec, Canada G1S 4L8, <sup>6</sup>Département de Psychiatrie, Université Laval, Québec, Québec, Canada G1K 7P4, and <sup>7</sup>Montreal Neurological Institute, McGill University, Montreal, Québec, Canada H3A 2B4

Adult neuronal precursors retain the remarkable capacity to migrate long distances from the posterior (subventricular zone) to the most anterior [olfactory bulb (OB)] parts of the brain. The knowledge about the mechanisms that keep neuronal precursors in the migratory stream and organize this long-distance migration is incomplete. Here we show that blood vessels precisely outline the migratory stream for new neurons in the adult mammalian forebrain. Real-time video imaging of cell migration in the acute slices demonstrate that neuronal precursors are retained in the migratory stream and guided into the OB by blood vessels that serve as a physical substrate for migrating neuroblasts. Our data suggest that endothelial cells of blood vessels synthesize brain-derived neurotrophic factor (BDNF) that fosters neuronal migration via p75NTR expressed on neuroblasts. Interestingly, GABA released from neuroblasts induces Ca<sup>2+</sup>-dependent insertion of high-affinity TrkB receptors on the plasma membrane of astrocytes that trap extracellular BDNF. We hypothesize that this renders BDNF unavailable for p75NTR-expressing migrating cells and leads to their entrance into the stationary period. Our findings provide new insights into the functional organization of substrates that facilitate the long-distance journey of adult neuronal precursors.

## Introduction

Since the discovery of neuronal progenitors in the adult brain approximately four decades ago (Altman and Das, 1966; Hinds, 1968), a key question in the field has been how these neuronal precursors migrate long distances, through complex brain territories, from the posterior to the most anterior parts of the brain. Neuronal precursors are generated in the subventricular zone (SVZ) and migrate first tangentially, in chains, along the rostral migratory stream (RMS) and, once in the olfactory bulb (OB), turn to migrate radially and individually out of the RMS into the

bulbar layer (Alvarez-Buylla and Garcia-Verdugo, 2002; Lledo and Saghatelyan, 2005).

Molecular signals that are involved in tangential migration of neuroblasts in the adult brain include the following: polysialated neural cell adhesion molecule (PSA-NCAM) (Cremer et al., 1994; Ono et al., 1994; Hu et al., 1996); members of the Slit (Wu et al., 1999); ephrin-B (Conover et al., 2000) and integrin families (Muras and Horwitz, 2002; Belvindrah et al., 2007); astrocyte-derived factor of unknown identity (Mason et al., 2001); the ErbB4 (Anton et al., 2004) and prokineticin 2 (Ng et al., 2005) receptors and neuroblast-derived GABA (Bolteus and Bordey, 2004). Reelin and tenascin-R, two extracellular matrix molecules, contribute to radial migration of neuronal precursors (Hack et al., 2002; Saghatelyan et al., 2004). Despite the extensive investigation of the molecular signals involved in the neuronal migration in the adult brain, our knowledge of how the RMS is defined and how neuronal precursors find their routes toward and into OB remains incomplete.

The most widely accepted model accounting for neuronal precursor migration posits that cell movements are dictated by chemorepulsive and chemoattractive gradients. Thus, neuroblasts are forced to remain in the migratory stream as a result of the action of chemorepellent molecules secreted from neighboring

Received Oct. 14, 2008; revised Feb. 5, 2009; accepted Feb. 6, 2009.

This work was supported by Canada Foundation for Innovation (CFI), Parkinson Society Canada, and Canadian Institutes of Health Research (CIHR) grants (A.S.). A.S. is a recipient of a Canada Research Chair in postnatal neurogenesis. We thank Drs. S. Nakamura (National Institute of Neuroscience, Tokyo, Japan), E. Castren (University of Helsinki, Helsinki, Finland) for providing BDNF plasmids, Dr. M. Kojima (National Institute of Advanced Science and Technology, Ikeda, Japan) for providing BDNF–GFP plasmid, Dr. J. Lee (Harvard Gene Therapy Initiative, Harvard Medical School, Boston, MA) for providing defective retroviral vector pMMP–fz–IRES–EGFP, and Drs. Freda Miller, Alain Trembleau, and Isabelle Caille for the comments on a previous version of this manuscript.

\*M.S. and M.L. contributed equally to this work.

Correspondence should be addressed to Armen Saghatelyan, Centre de Recherche Université Laval Robert-Giffard, Université Laval, 2601 Chemin de la Canadière, Québec, Québec, Canada G1J 2G3. E-mail: armen.saghatelyan@crulrg.ulaval.ca.

DOI:10.1523/JNEUROSCI.4956-08.2009

Copyright © 2009 Society for Neuroscience 0270-6474/09/294172-17\$15.00/0

territories, such as Slit released from the septum (Wu et al., 1999) and choroid plexus (Sawamoto et al., 2006), and are guided by chemoattractive molecules secreted from the OB that include prokineticin 2 (Ng et al., 2005) and glial cell line-derived neurotrophic factor (Paratcha et al., 2006). However, surgical removal of the OB does not abolish neuronal migration (Jankovski et al., 1998; Kirschenbaum et al., 1999), suggesting that molecules secreted from the OB are not essential for neuroblasts migration in the adult RMS (Marín and Rubenstein, 2003). Furthermore, the migratory pathway of newborn cells in the adult brain has very complex curvature architecture and numerous chemorepellent molecule gradients acting in concert and with different efficiency would be required to ensure a faithful migration.

In the studies presented here, we have tested the hypothesis that neuroblasts migrate along physical substrates that topographically define the RMS. We show that blood vessels precisely outline the migratory stream for new neurons from the posterior (SVZ) to the most anterior (OB) regions of the adult brain and that they serve as a physical substrate for migrating neuroblasts in the adult brains. We identify brain-derived neurotrophic factor (BDNF) as a molecular signal that is released from endothelial cells of blood vessels and show that it fosters neuronal migration via p75NTR activation on neuroblasts. Interestingly, GABA released from neuroblasts leads to the insertion of high-affinity TrkB receptors on the plasma membrane of astrocytes that ensheath neuronal precursors and contact blood vessels. Consequently, astrocytes trap free extracellular BDNF. We hypothesize that, via this mechanism, neuroblasts control the amount of extracellular BDNF and, therefore, the periodicity of the migratory periods. Together, our data provide functional and mechanistic explanations for long-distance journey of new cells in the adult brain. This information may contribute to the development of new strategies to cure neurodegenerative diseases and brain trauma.

## Materials and Methods

**Animals.** All experiments were performed in adult 2- to 3-month-old C57BL/6 mice (Charles River), GAD67–green fluorescent protein (GFP)-deficient mice (Ono et al., 2005), and p75NTR-deficient mice (Lee et al., 1992) in accordance with Laval Institute guidelines. TrkB floxed mice (Minichiello et al., 1999) were crossed with *GlastCre::ERT2* mice (Mori et al., 2006), which carry an inducible form of Cre in the astrocyte-specific glutamate transporter (GLAST) locus. As experimental animals, *TrkB<sup>fl/fl</sup> GLAST::CreERT2* and control *TrkB<sup>wildtype/wildtype</sup> GLAST::CreERT2* were used. Two- to 3-month-old mice received intraperitoneal injections of 1 mg of Tamoxifen, two injections per day for 5 consecutive days (Mori et al., 2006). To evaluate the proportion of cells that underwent recombination, *GLAST::CreERT2* mice were crossed with reporter mice (*Z/EG*). Animals were kept on a 12 h light/dark cycle at constant temperature (22°C) with food and water *ad libitum*.

**Stereotaxic injections and osmotic minipump infusions.** To label newborn neurons, GFP-encoding retrovirus was injected either to the SVZ (for analysis of cell migration in the RMS) or to the RMS (for analysis of cell migration in the OB) at the following coordinates (in mm): for the SVZ, anteroposterior, 0.75; mediolateral, 1.20; dorsoventral, 1.9; and for the RMS, anteroposterior, 2.55; mediolateral, 0.82; dorsoventral, 2.9. BDNF (100 ng; Peprotech) and vehicle (NaCl, 0.9%) were injected stereotaxically to the striatum at the following coordinates (in mm): anteroposterior, 0.9; mediolateral, 0.8; dorsoventral, 2.1. IgG–Fc, TrkB–Fc (10 µg/ml; 100 µl infusion volume; R & D Systems), and function-blocking antibodies for p75NTR described previously (Clary and Reichardt, 1994) were infused via 7 d osmotic minipumps (Alzet) at the following coordinates (in mm): anteroposterior, 2.55; mediolateral, 0.82; dorsoventral, 2.7. Double-stranded siSTABLE small interfering RNAs (siRNA) directed against BDNF mRNA were obtained from Dharmacon. In addition,

FITC fluorescent tag was added to 5' end of siRNA. The sense and antisense sequences of BDNF were designed as follows: sense, GAAC-TACCCAATCGTATGTTTT; antisense, ACATACGATTGGGTAGT-TCTT. BDNF siRNA and control siRNA were infused via 7 d osmotic minipump directly to the external carotid artery. For this, mouse jugular catheter (Alzet) connected to the osmotic minipump was inserted to the external carotid artery and maintained in place with non-absorbable silk sutures. Heparin at 5 µl was added to 100 µl of solution containing either control or BDNF siRNAs.

**Immunohistochemistry and in situ hybridization.** Immunohistochemistry was performed as described previously (Saghatelian et al., 2004). The following antibodies were used: rabbit (N-20; 1:50; Santa Cruz Biotechnology), goat (K-14; 1:50; Santa Cruz Biotechnology), and chicken (1:50; Promega) anti-human BDNF; goat anti-human (N-20; 1:50; Santa Cruz Biotechnology) and rabbit anti-mouse (1:1000; Millipore Bioscience Research Reagents) TrkB; rabbit anti-human (H-137; 1:50; Santa Cruz Biotechnology) and anti-rat (1:500; Covance and 1:500; Millipore) p75NTR; guinea-pig anti-mouse doublecortin (1:1000; Abcam); mouse anti-PSA-NCAM (1:1000; Millipore Bioscience Research Reagents); mouse anti-5-bromo-2'-deoxyuridine (BrdU) (1:200; Serotec); rabbit (1:1000; Dako) and mouse (1:1000; Millipore Bioscience Research Reagents) anti-GFAP; rabbit anti-caspase 3 (1:500; Cell Signaling Technology); and rabbit anti-Ki67 (1:1000; Abcam) and rat anti-mouse platelet/endothelial cell adhesion molecule (PECAM) (1:1000; BD Pharmingen). For some immunostainings, we used tyramide amplification kit (PerkinElmer Life and Analytical Sciences). The DNA synthesis marker BrdU (Sigma) was dissolved in a sterile solution of 0.9% NaCl and 1.75% NaOH (0.4 N). This solution was injected intraperitoneally at a concentration of 50 mg/kg body weight. Two injections of BrdU spaced 2 h apart were performed 5 d before killing the animals to evaluate the number of BrdU-positive (BrdU<sup>+</sup>) in the RMS<sub>OB</sub>. For osmotic minipump infusion of IgG–Fc, TrkB–Fc, and function-blocking antibodies for p75NTR above the horizontal limb of RMS, BrdU was injected twice spaced by 2 h 2 d before installation of pumps. One pulse of BrdU was given 6 h before installation of pumps to the carotid artery. BrdU staining was performed as described previously (Saghatelian et al., 2004), and BrdU<sup>+</sup> cells were counted in each third 40-µm-thick section. In some experiments, blood vessels were visualized by injecting fluorescent dextran (molecular weight, 70,000 kDa) to the tail vein. Corresponding secondary antibodies were used. Images were acquired with an FV1000 confocal microscope equipped with argon 488 nm, helium–neon 543 nm, and helium–neon 633 nm lasers (Olympus). Double- and triple-immunolabeled cells were analyzed using three-dimensional (3D) reconstructed images with the *x–z* and *y–z* orthogonal projections.

For *in situ* hybridization studies, antisense RNA probes were labeled using the DIG RNA labeling kit (Roche Diagnostics) and purified on ProbeQuant G-50 columns (GE Healthcare). *In situ* hybridization was performed on 50-µm-thick vibratome sections, and the signals were revealed with nitroblue-tetrazolium-chloride/5-bromo-4-chlor-indolyl-phosphate (Promega). Antisense RNA probes were obtained from plasmids containing a fragment of the extracellular domain of mouse TrkB (kindly provided by Dr. Lino Tessarollo, National Institutes of Health, Bethesda, MD) and two plasmids containing mouse BDNF [kindly provided by Drs. S. Nakamura (National Institute of Neuroscience, Tokyo, Japan) and E. Castren (University of Helsinki, Finland)].

**Retrovirus production.** The replication defective retroviral vector pMMP–f2–IRES–EGFP (obtained from Dr. J. Lee, Harvard Gene Therapy Initiative, Harvard Medical School, Boston, MA) was produced by calcium phosphate-mediated transfection of the vector DNA into the retrovirus-packaging cell line GPG-293 and was subsequently concentrated from the supernatant by ultracentrifugation. Titration was performed by infecting NIH-3T3 cells with serial dilutions of the vector and counting the number of enhanced GFP (EGFP)-positive cells or colonies 72 h after infection.

**Slice preparation and time-lapse video imaging.** Sagittal sections (250 µm) from adult (2–3 months old) mouse forebrain were prepared and maintained at 32°C. Slices were continually superfused (2 ml/min) with artificial CSF (ACSF) containing the following (in mM): 125 NaCl, 26 NaHCO<sub>3</sub>, 10 glucose, 3 KCl, 2 CaCl<sub>2</sub>, 1.3 MgCl<sub>2</sub>, and 1.25 NaH<sub>2</sub>PO<sub>4</sub>.

(bubbled with 95% O<sub>2</sub>/5% CO<sub>2</sub>), pH ~7.4. For Ca<sup>2+</sup> imaging of astrocytes, slices were incubated for 1 h with 2 μM Fluo4-AM, a membrane-permeable Ca<sup>2+</sup> indicator. For time-lapse video imaging of cell migration and Ca<sup>2+</sup> fluctuation in astrocytes, multiple z-stack images (at least 6–10 z-sections, with ~10 μm interval) were acquired every 15 s for at least 1 h with a BX61WI (Olympus) upright microscope equipped with CCD camera (CoolSnap HQ2). For Ca<sup>2+</sup> imaging experiments, Fluo4 was excited by using a DG-4 xenon light source (Sutter Instruments). At least 20 migrating cells were analyzed per slice and for each time point. Multiple z-step acquisition in our time-lapse experiments of cell migration allowed us to follow the same cell in different z plans. For the analysis of stationary periods, we took into consideration only those phases that were intercepted by two migratory periods. For the experiments requiring pharmacological treatment (BDNF, antibodies, GABA, bicuculline, etc.), time-lapse movies were first acquired under control conditions for 30–45 min and then in the presence of the pharmacological agent for another 30–45 min. Under these conditions, we were unable to see long stationary phases (intercepted by two migratory periods), and, therefore, our values for stationary periods are shorter compared with the ones obtained from 1.5–2 h of recordings (see Fig. 2F). At least 50 time points were averaged for each slice to obtain the mean value for the changes induced by pharmacological agent. Control values were calculated by averaging 50 time points before drug application. These values were than averaged across all slices. Because of low amounts of p75NTR function-blocking antibodies, we incubated the slices with these antibodies for 1 h before recording. For time-lapse video imaging of GFP<sup>+</sup> neuroblasts along dextran–Texas Red-labeled blood vessels, imaging was performed deep in the slice (40–100 μm from the slice surface).

**Fluorescence-activated cell sorting and neurosphere analysis.** SVZ was dissected from five animals, and tissue was dissociated to the single cells. Single-cell suspension was incubated with rabbit anti-rat p75NTR (1:200; Millipore) on ice for 20 min and then washed with PBS containing 1% fetal calf serum (FCS). Anti-p75NTR binding was detected with Alexa 647-coupled anti-rabbit IgG (1:500; Invitrogen). Before sorting, cells were washed with PBS containing 0.5 μg/ml propidium iodide to exclude dead cells. Cells were sorted on a FACSAria (BD Biosciences) and collected into the medium containing epidermal growth factor (EGF) and basic fibroblast growth factor (FGF). Sorted cells were plated into 96-well tissue culture plates at density of one cell per well, as confirmed by counting 4 h after plating, in FGF (10 ng/ml) and EGF (20 ng/ml) containing medium. After 7 d of culturing, neurosphere formation was used as a readout for proliferative activity of p75-positive and p75-negative cell populations. The identity of the sorted cells was assessed immediately after the sorting. Namely, 1000 fluorescence-activated cell sorting (FACS) events have been cytopinned, cells were fixed in 4% paraformaldehyde and stained for doublecortin (Dcx) (rabbit antibody; 1:200; Millipore) and GFAP (rabbit antibody; 1:200; Dako) visualized by the secondary anti-rabbit antibodies coupled with cyanine 2 and 3, respectively.

**Reverse transcription-PCR analysis of FACS-purified cell populations.** SVZ was dissected from five hGFAP–EGFP transgenic mice per experiment, and tissue was dissociated to the single cells. The following cell populations were purified using FACS: astrocytes (GFP-positive, PSA-NCAM-negative population), neuroblasts (PSA-NCAM-positive population, mouse IgM, 1:100), and endothelial cells (vascular endothelial cadherin-positive cells, mouse IgG, 1:400) as described above. Immediately after the sorting, the total RNA was isolated from the different populations using RNeasy Micro kit (Qiagen), according to the instructions of the manufacturer. First-strand cDNA synthesis reaction was performed with RevertAid H Minus First Strand cDNA Synthesis kit (Fermentas Life Science) with oligo-dT primers. Obtained cDNA were amplified using the following primers: for BDNF, 5'-CAACATAA-ATCCACTATCTTC-3' and 5'-ATGACCATCCTTTCTTAC-3'; for TrkB, 5'-TGAAGACGCTGAAGGACGCCA-3' and 5'-CAGGTTCTCCTACCAAGCA-3'; for p75NTR, 5'-CCAGCAGACCACACACACAGACTG-3' and 5'-CCCTACACAGAGATGCTCGGTTCT-3'; for glyceraldehyde-3-phosphate dehydrogenase, 5'-TCCCATTCTCC-ACCTTTGATG-3' and 5'-GTCCACCACCCTGTTGCTGA-3'; and for β-actin, 5'-CACCCTTCTACAATGAGC-3' and 5'-CGGTACGATCTTCATGAGG-3'.

**Primary culture of adult astrocytes.** To prepare culture of astrocytes from the adult SVZ, the lateral wall of the lateral ventricle from the brains of at least five 6- to 9-week-old C57BL/6 mice were dissected out under a microscope. Preparation was performed in HBSS containing 10 mM HEPES. The isolated brain tissue was then centrifuged and resuspended in 10 ml of culture medium. Cells were cultured under adherent conditions in the presence of 10% fetal bovine serum, 5% horse serum, DMEM/F-12 supplemented with B27 and growth factors (20 ng/ml EGF and 10 ng/ml FGF2). Medium was changed every second day. For ELISA experiments, astrocytes were seeded on poly-D-lysine-coated coverslips in six-well plates. For coculture of astrocytes and endothelial cells, astrocytes were prepared as described, and then human umbilical vein endothelial cells (HUVECs) transfected with BDNF–GFP plasmid (kindly provided by Dr. M. Kojima, National Institute of Advanced Science and Technology, Ikeda, Japan) were added. The cocultures were analyzed 24 h later with the help of FV1000 confocal microscope (Olympus). After control acquisition of GFP<sup>+</sup> punctate labeling on the surface of astrocytes, a small region of interest was selected and bleached for 1 min with an argon 488 nm laser. Astrocytes were visualized in bright-field images according to their large soma size and were identified with *post hoc* staining with GFAP antibodies.

**Isolation of fibroblasts and endothelial cells.** Human fibroblasts were isolated from skin biopsies after breast reductive surgeries as described previously (Berthod et al., 2006) using 0.2 IU/ml collagenase H (Roche Diagnostics). Cells were grown in DMEM (Invitrogen) supplemented with 10% FCS (HyClone), 100 IU/ml penicillin G (Sigma), and 25 mg/ml gentamicin (Schering) and incubated in 8% CO<sub>2</sub> at 37°C. HUVECs were obtained from healthy newborns by enzymatic digestion with 0.250 mg/ml thermolysin (Sigma) as described previously (Berthod et al., 2006). They were grown in endothelial growth medium-2 (EGM-2; Cambrex Bioscience Baltimore) and characterized as described previously (Berthod et al., 2006).

**Construction of the tissue-engineered 3D capillary-like network.** Collagen-chitosan sponges were used as a scaffold to construct a 3D capillary-like network as described previously (Berthod et al., 2006). Briefly, type I and III bovine collagen (Symatase) and chitosan (Kemestrie) were dissolved and mixed in 0.1% acetic acid, and 1 ml/well (3.8 cm<sup>2</sup>) of the final solution was poured in 12-well plates (BD Biosciences), frozen at –80°C, and lyophilized in a vacuum lyophilizer (Dura-Stop Freeze-Dryer; FTS Systems). Human dermal fibroblasts and HUVECs (2.1 × 10<sup>5</sup> cells/cm<sup>2</sup> each) were seeded on top of the sponges and cultured for 10 d in a 1:1 ratio of EGM-2/DMEM, supplemented with 75 μg/ml ascorbic acid. The sponges were cultured in a 3:1 ratio of DMEM/Ham's F-12 medium supplemented with 10% FBS, 0.4 μg/ml hydrocortisone, 5 μg/ml bovine insulin, 100 μg/ml ascorbic acid, and antibiotics and were elevated to the air–liquid interface for 17 additional days.

For time-lapse imaging of migrating neuroblasts in the reconstituted 3D capillary-like network, GFP<sup>+</sup> cells derived from the SVZ of GAD67–GFP mice were cultured together with HUVECs and fibroblast prepared sponges. In control experiments, GFP<sup>+</sup> neuroblasts were cultured with sponges prepared from fibroblasts alone. HUVECs were transfected with GFP lentivirus. GFP<sup>+</sup> neuroblasts (small cells of ~5–10 μm size) and GFP<sup>+</sup> capillaries (long tubular-like structures) were easily distinguishable on the basis of their shapes and were false-colored in offline analysis using ImagePro software (see Fig. 6L).

For reconstituted capillaries, siRNA transfection were performed with HiPerFect transfection reagent (Qiagen) according to the instructions of the manufacturer. BDNF and control siRNAs were provided from Santa Cruz Biotechnology (sc-42121 and sc-37007, respectively). BDNF siRNA were a pool of three target-specific 20–25 nt siRNA designed to knock down BDNF gene expression. Control siRNA were a nontargeting siRNA designed as negative control. Each transfection was effectuated with 70 μM of siRNA. Total RNA was prepared using the Invitrogen TRIzol reagent according to the instructions of the manufacturer. siRNA efficiency were checked by reverse transcription (RT)–PCR reaction with the primers provided from Santa Cruz Biotechnology (sc-42121-Pr).

**Determination of BDNF concentration.** The primary culture of astrocytes from adult SVZ were treated with GABA (10 μM) for 30 min. The total protein concentration was determined by Bradford assay (Bio-

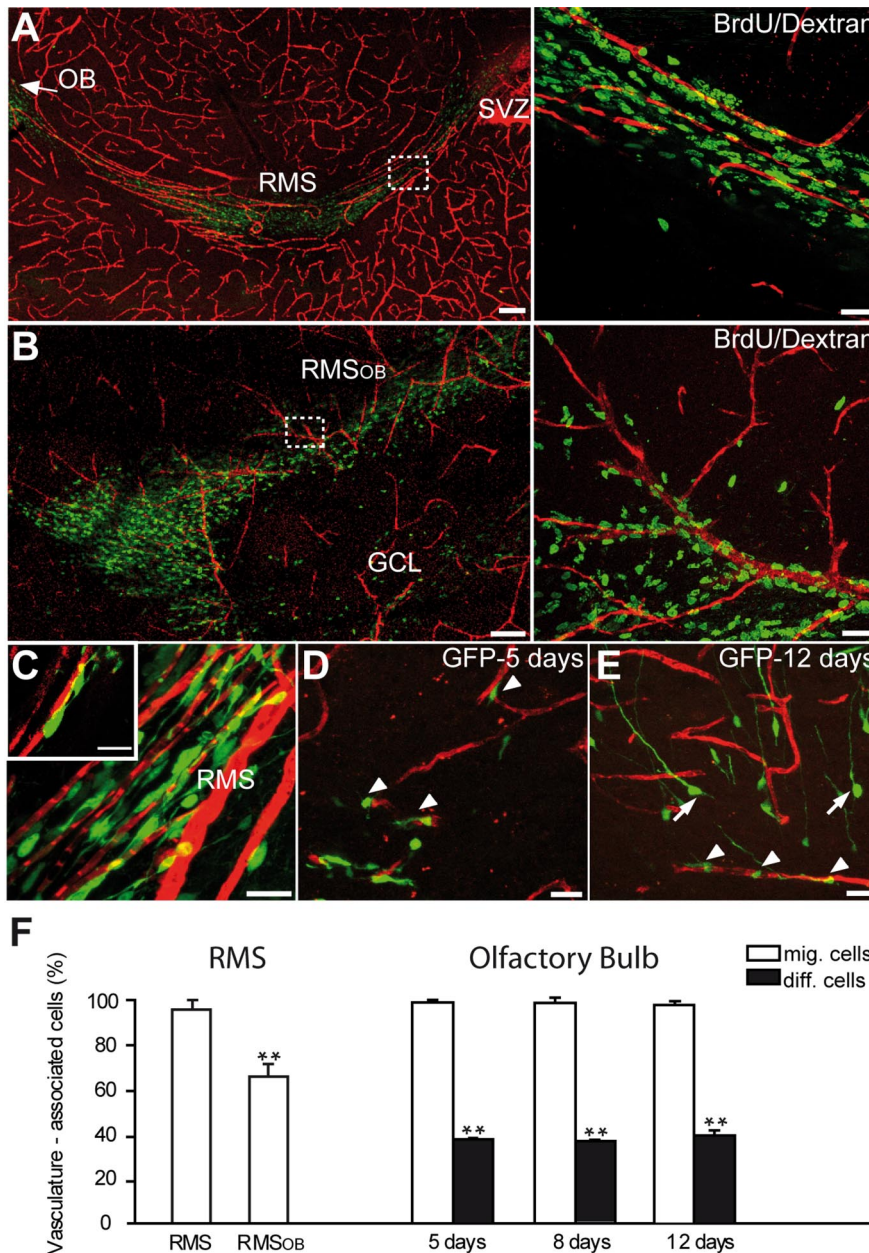


**Figure 1.** Migrating neuroblasts are aligned along the blood vessels in the adult brain. *A, B*, Micrographs showing organization of blood vessels in the adult mouse forebrain. Note the close association of tangentially (*A*) and radially (*B*) migrating neuronal precursors (green) with blood vessels (red) that parallel the migratory stream. Newly generated cells in the migratory pathway were labeled by BrdU injection 5 d before analysis. Blood vessels were revealed by injection of dextran–Texas Red to the tail vein. Scale bars: *A, B*, 100  $\mu$ m; *A<sub>right</sub>, B<sub>right</sub>*, 20  $\mu$ m. *C–E*, Vasculature-associated GFP<sup>+</sup> cells in the RMS and OB. GFP-expressing retrovirus was injected into the SVZ (*C*) or RMS (*D, E*) 5, 8, and 12 d before analysis. Arrowheads and arrows indicate migrating (mig.) and differentiating (diff.) cells, respectively. Scale bars, 10  $\mu$ m. *F*, Quantification of vasculature-associated cells in the RMS and OB.

Rad), and BDNF concentration was measured by BDNF E<sub>max</sub> Immuno-Assay system (Promega) according to the protocol of the manufacturer. Exogenous BDNF (10 ng/ml) was added to the cultures for 30 min, and then cultures were washed extensively and treated with GABA as described.

**Surface TrkB internalization.** TrkB internalization was evaluated by biotinylation of surface TrkB receptors. Acute slices of the adult mouse forebrain were incubated in bicuculline (100  $\mu$ M), GABA (10  $\mu$ M), or BDNF (10 ng/ml) for 1 h. After incubation, slices were immediately transferred to ice-cold HBSS, and the RMS and SVZ were extracted under a dissecting microscope. The cells were dissociated, washed in ice-cold PBS, and biotinylated

with EZ-Link Sulfo-NHS-biotin (Pierce) for 30 min according to the protocol of the manufacturer. The cells were then extensively washed with ice-cold PBS containing 100 mM glycine and lysed using a buffer containing the following (in mM): 50 Tris-HCl, 1 EDTA, 1 EGTA, 1 sodium orthovanadate, 50 sodium fluoride, 5 sodium pyrophosphate, 10 sodium b-glycerophosphate, 0.1% 2-mercaptoethanol, 1% Triton X-100, and a 1:100 dilution of freshly added protease inhibitor cocktail set III (Calbiochem). The biotinylated surface proteins were immobilized on streptavidin-coated agarose beads (GE Healthcare), incubated with anti-TrkB antibodies, followed by incubation with HRP-labeled secondary antibodies. HRP-labeled TrkB immunocomplexes were eluted in 0.1 M glycine-HCl, and surface TrkB protein concentrations were determined by ELISA.

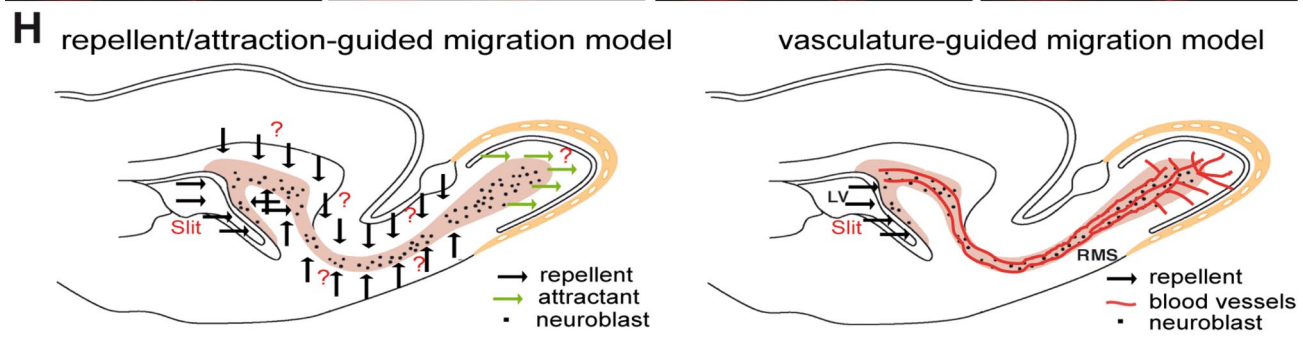
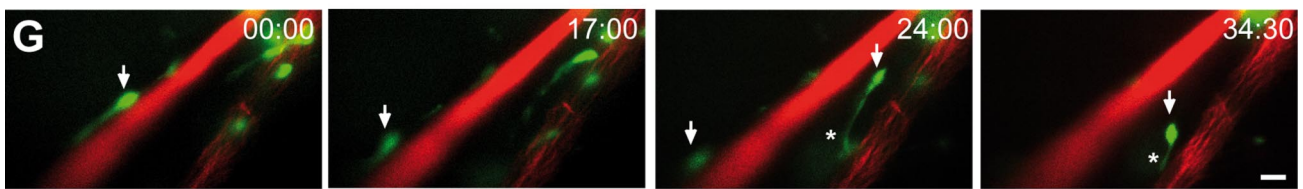
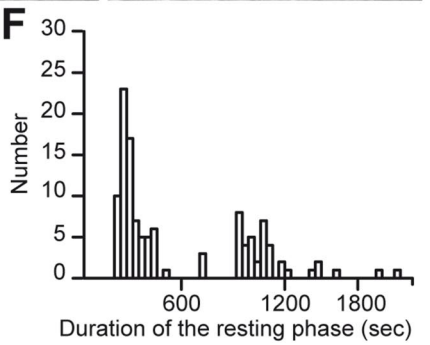
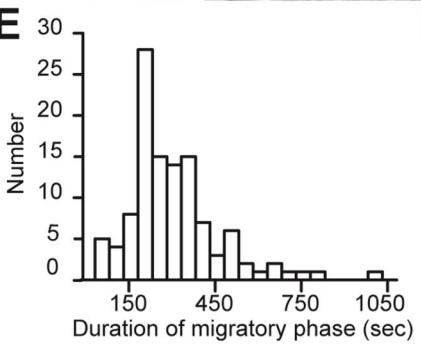
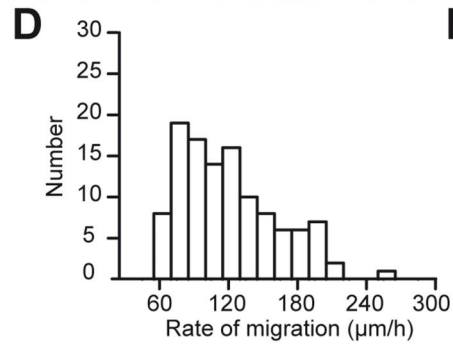
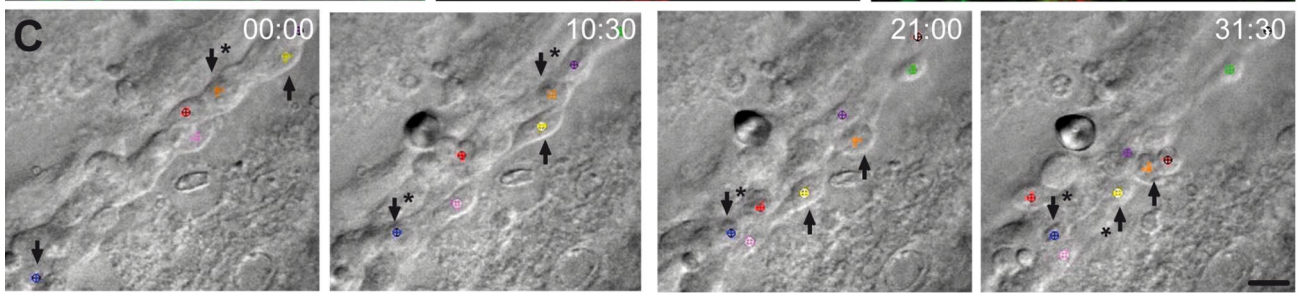
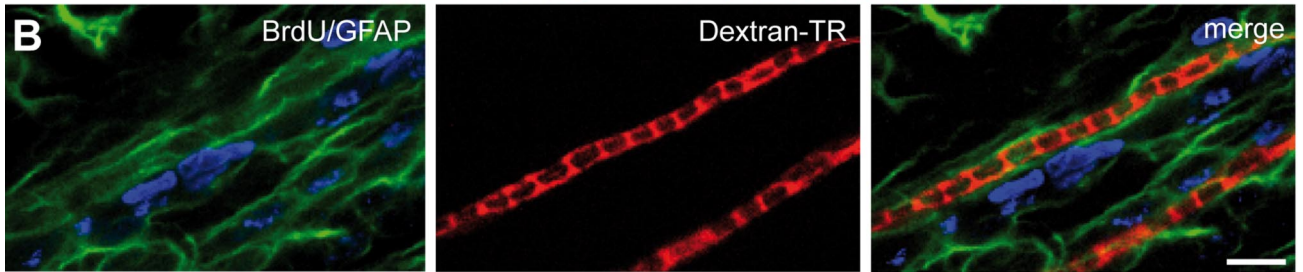
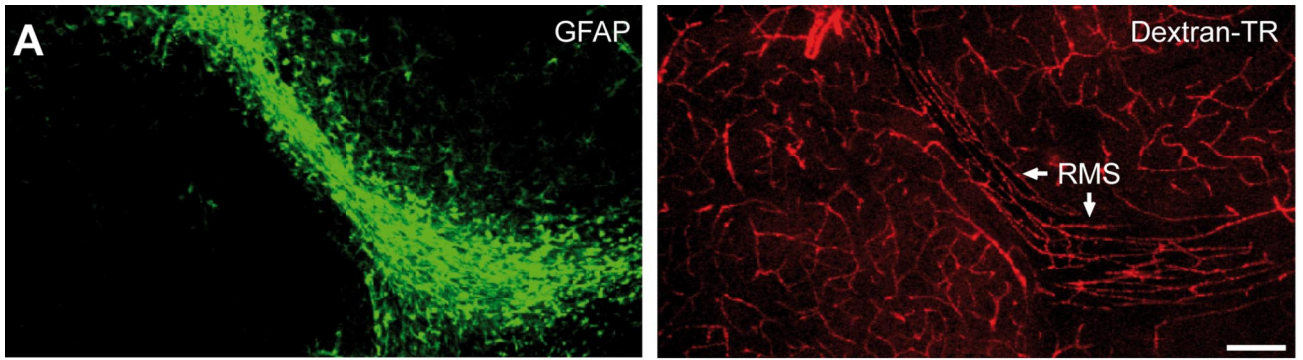
**Statistical analysis.** Data are presented as mean  $\pm$  SEM. Statistical significance was tested by using Student’s *t* test (with \**p* < 0.05 and \*\**p* < 0.001).

**Results**

**Adult neuronal precursors are aligned and migrate along the blood vessels**

To investigate whether the SVZ–OB pathway contains physical substrates that might be used by neuronal precursors for their faithful migration from the posterior to the most anterior parts of the brain, we performed blood vessel labeling in the adult mammalian forebrain. When blood vessels were labeled via injection of fluorescent dextran–Texas Red into the tail vein or by immunohistochemical detection for PECAM, a marker of endothelial cells, an unexpected organization of blood vessels was observed in the SVZ–OB pathway. Blood vessels in most parts of the brain are distributed in a rather random manner, but, in the RMS, they parallel the migratory stream and almost all migrating cells are aligned along the blood vessels (Fig. 1*A*) (supplemental Video 1, available at [www.jneurosci.org](http://www.jneurosci.org) as supplemental material). Interestingly, blood vessel organization is modified in the core of the OB, in which neuroblasts have to detach from each other and start to migrate radially. Whereas some blood vessels are still oriented parallel to the migratory stream and reach the most rostral end of the RMS of OB (RMS<sub>OB</sub>), many others are organized perpendicularly with respect to the tangentially migrating neuroblasts (Fig. 1*B*).

Moreover, cells that exit from the RMS<sub>OB</sub> and initiate their radial migration into the bulbar layers do so along these perpendicularly oriented blood vessels (Fig. 1*B*). Quantification of the number of BrdU-labeled migrating cells (to reveal migrating cells, BrdU was injected 5 d before counting) along the blood vessels revealed that, among 444 BrdU-labeled cells, 75.3  $\pm$  4.1% of them were within 3  $\mu$ m of blood vessels (*n* = 3 animals). Because BrdU labeling depicts only cell nuclei and not the cell body or processes, these numbers likely underrepresent the proportion of



blood vessel-associated neuroblasts. Therefore, we counted the number of vasculature-associated neuroblasts whose soma or leading process could be easily identified in either GAD67–GFP transgenic animals or animals in which a GFP-encoding retrovirus was injected into the SVZ. Among 921 GFP<sup>+</sup> cells counted in the RMS, 97.3 ± 0.7% of neuroblasts were located within 3 μm of blood vessels (*n* = 5 animals) (Fig. 1C,F). This number is decreased in the RMS<sub>OB</sub> in which neuroblasts have to change their mode of migration from tangential to radial. At this level, 33.3 ± 4.9% of GFP<sup>+</sup> neuroblasts were “detached” from blood vessels (Fig. 1F; see also B). However, only vasculature-associated neuronal-specific nuclear protein-negative migrating cells are found in the OB at 5, 8, and 12 d after stereotaxic RMS injection of GFP-encoding retrovirus (99.4 ± 1.2%, *n* = 161 cells from 4 animals, at 5 d; 98.9 ± 2.0%, *n* = 91 cells from 5 animals, at 8 d; and 98.3 ± 1.7%, *n* = 93 cells from 4 animals, at 12 d) (Fig. 1D–F). After their arrival to the OB, newborn cells that start to differentiate and develop long dendritic processes (>30 μm) were equally abundant close to or distant from blood vessels (Fig. 1E,F).

To determine whether migrating cells physically contact blood vessels, we performed coimmunostains for BrdU-labeled neuroblasts, for vasculature, and for astrocytes (Fig. 2A,B), which are known to ensheath migrating cells (Alvarez-Buylla and Garcia-Verdugo, 2002; Lledo and Saghatelian, 2005). Analysis of sections after triple immunolabeling revealed that blood vessels are enveloped by the processes of GFAP-expressing astrocytes and that BrdU- or Dcx-labeled migrating cells are attached to these processes (Fig. 2B). These data revealed that adult neuroblasts, enveloped by astrocytic processes, are positioned close (<3 μm away) to blood vessels, but they do not show whether these migrating cells use blood vessels as a scaffold for their migration. To investigate this issue, we decided to monitor migrat-

ing neuroblasts in real time. For this, we studied the behavior of migrating neuronal precursors in acute slices of the adult (2–3 months old) mouse forebrain with time-lapse video imaging. This analysis revealed fast migration of neuronal precursors in the RMS (121.2 ± 3.9 μm/h; *n* = 64 cells from 4 animals) (Fig. 2C,D) (supplemental Video 2, available at www.jneurosci.org as supplemental material). The migration of neuronal precursors was saltatory and comprised two distinct phases: displacement of neuronal cell body toward the leading process (288.1 ± 18.4 s; *n* = 64 cells from 4 animals) (Fig. 2E) separated by a resting period (492.3 ± 41.5 s; *n* = 64 cells from 4 animals) (Fig. 2F). To examine whether these migrating neuroblasts used blood vessels for their saltatory displacement, we imaged GFP-labeled neuronal precursors deep in the slices in which dextran–Texas Red-stained blood vessels preserve their integrity. Our time-lapse analysis revealed that 88.1 ± 4.6% of neuronal precursors migrate along blood vessels (<3 μm away during entire period of recording) in the adult RMS (*n* = 118 cells from 7 animals) (Fig. 2G) (supplemental Video 3, available at www.jneurosci.org as supplemental material). Even in the cases when the soma of GFP<sup>+</sup> neuroblasts migrate >3 μm away from the blood vessels, these cells almost invariably preserve their leading process close to blood vessels (Fig. 2G) (supplemental Videos 3,4, available at www.jneurosci.org as supplemental material). This type of migration is likely to be used under circumstances when migrating neuronal precursors meet some physical constrains (such as soma of astrocytes or neuroblasts in the stationary phase) that impede straightforward propagation along the blood vessel. Together, these data indicate that vasculature plays an important role in the migratory behavior of neuronal precursors in the RMS–OB pathway and that these migratory cells use blood vessels for their navigation in the adult brain (for a model, see Fig. 2H). But what are the mechanisms of this vasculature-associated migration?

←

**Figure 2.** Neuronal precursors migrate along the blood vessels in the adult brain. **A**, GFAP-labeled astrocytes (green) and dextran–Texas Red (TR)-labeled blood vessels (red) in the adult RMS. Note the parallel organization of blood vessels in the RMS. Scale bar, 100 μm. **B**, Micrographs of BrdU-positive cells (5 d after BrdU injection) in the close vicinity of dextran–Texas Red-loaded blood vessels (injection to the tail vein). GFAP-labeled astrocytes (green) envelop blood vessels (red), and neuroblasts (blue) are attached to the astrocytic processes. Scale bar, 10 μm. **C**, Time-lapse video imaging of migrating neuroblasts in slices from the adult mouse forebrain (time is indicated in minutes in the top right corner of each photograph). Migrating cells are indicated during their migratory (arrows only) and stationary (arrows with asterisks) phases. **D–F**, Rate of migration and durations of migratory and stationary periods of neuronal precursors in the RMS in the acute slices of mouse forebrain. **G**, GFP-labeled neuronal precursors migrate along blood vessels in the acute slices of the adult mouse forebrain. Blood vessels were labeled by injection of dextran–Texas Red to the tail vein 1 h before preparation of acute slices. GFP-expressing retrovirus was injected into the SVZ 3 d before time-lapse imaging in the RMS. Arrows indicate the soma of migratory cells, whereas asterisk shows leading process. Note that GFP<sup>+</sup> cells are always positioned close to the vasculature either with their soma or leading processes. Time is indicated in minutes in the top right corner of each photograph. Scale bar, 10 μm. **H**, Schematic representation of the adult brain showing the migratory pathway. According to the repellent/attraction-guided model, neuroblasts remain in this complex-shaped migratory stream because of myriads of chemorepellent molecules (black arrows) secreted from all RMS-neighboring territories and are guided toward OB attributable to chemoattractive molecules secreted from this region (green arrows). According to the vasculature-guided migration model proposed herein, neuroblasts are retained in the RMS and migrate in this pathway as a result of the presence of blood vessels that are oriented parallel to the migratory stream. Neuroblasts course along blood vessels, and a single chemorepellent molecule that is secreted from the posterior parts of the brain could be sufficient to direct neuronal precursors to the OB. Neuroblasts receive all other signal(s) for their migration from RMS–OB vasculature. It should be noted, however, that the vasculature-guided migration model proposed here does not exclude the earlier chemorepellent/chemoattraction-mediated scheme. It is likely that both mechanisms operate in parallel to ensure faithful migration of newborn cells in the adult brain.

### Mechanisms of vasculature-associated migration

Endothelial cells synthesize BDNF (Leventhal et al., 1999; Louis-saint et al., 2002; Guo et al., 2008), injection of this trophic factor into the lateral ventricle leads to the appearance of new neurons in the parenchyma of the striatum (Benraiss et al., 2001; Pencea et al., 2001; Bédard and Parent, 2004) (but see also (Galvão et al., 2008)), and it has been suggested recently that BDNF affects migration of neuronal precursors in the RMS (Chiamarello et al., 2007; Bath et al., 2008). We therefore tested the putative role of BDNF in the vasculature-guided migration of neuronal precursors. *In situ* hybridization analysis for BDNF combined with immunohistochemistry for PECAM showed BDNF mRNA expression in the endothelial cells of blood vessels in the adult RMS (Fig. 3A). In contrast, astrocytes and neuroblasts in the RMS were devoid of BDNF mRNA (Fig. 3A) (supplemental Fig. 1, available at www.jneurosci.org as supplemental material). Semiquantitative RT-PCR analysis of FACS-purified endothelial cells, astrocytes, and neuroblasts confirmed the presence of BDNF mRNA in the endothelial cells but not in other cells types of the adult migratory pathway (*n* = 3 experiments) (Fig. 3B). Interestingly, however, immunodetection of BDNF revealed a different distribution with the protein mostly found on the astrocytic processes enveloping blood vessels (Fig. 3C). To confirm that our immunostaining reflects the actual presence of BDNF protein, immunostains were also performed on sections derived from TrkB–Fc-infused animals. Application of TrkB–Fc (10 μg/ml) via 7 d osmotic minipump implants placed just above the horizontal limb of the RMS, to capture endogenous BDNF, decreased the

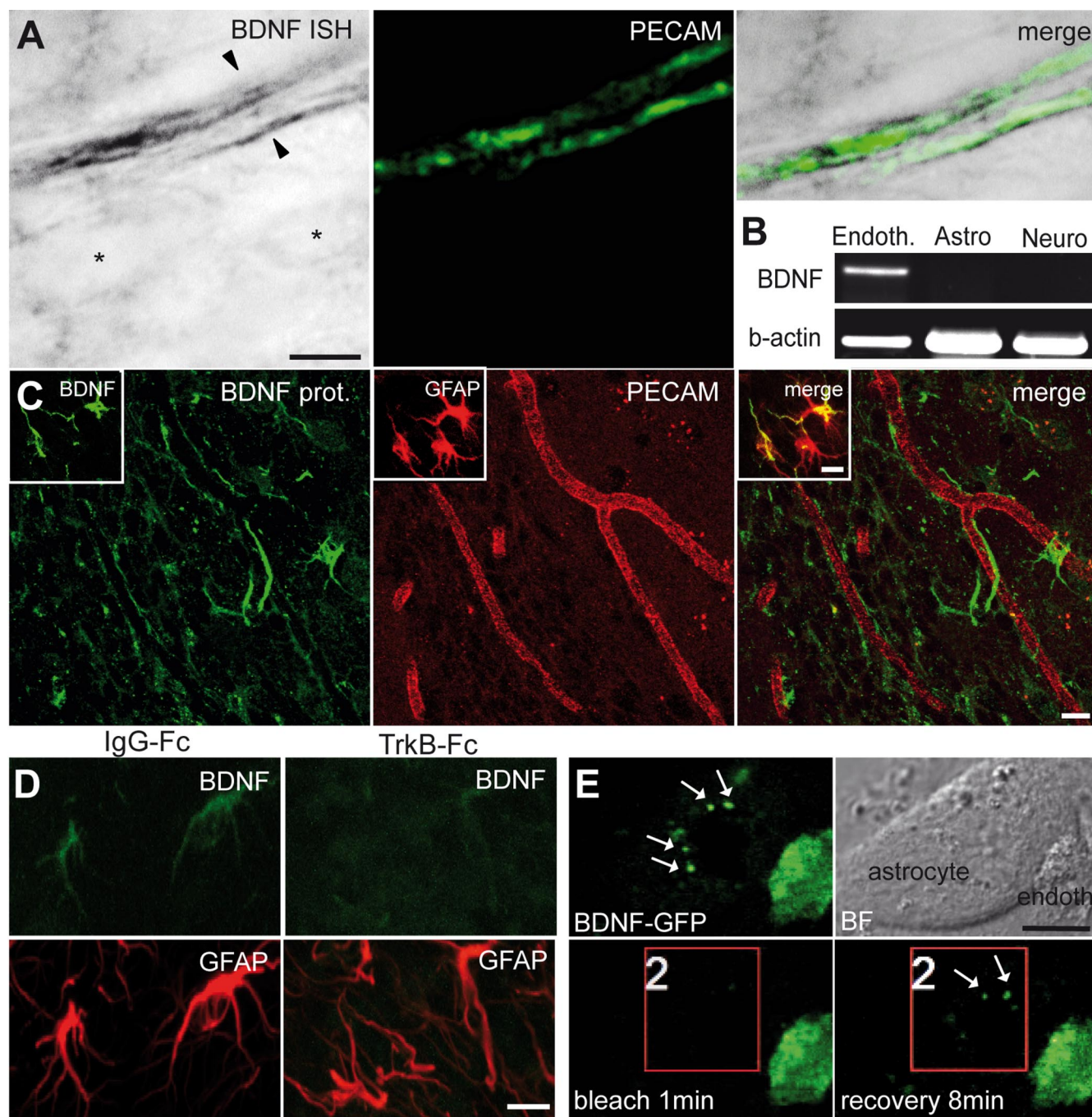


**Figure 3.** Expression of BDNF in the adult RMS. *A*, *In situ* hybridization (ISH) for BDNF and immunostaining for PECAM (green) showing that endothelial cells of blood vessels synthesize BDNF. Note that BDNF mRNA is present in the endothelial cells (arrowheads) but not in other cell types of the adult RMS (asterisks). Scale bar, 5  $\mu$ m. *B*, RT-PCR analysis of FACS-purified endothelial cells (Endoth.), astrocytes (Astro), and neuroblasts (Neuro). BDNF is expressed in endothelial cells but not in astrocytes and neuroblasts. *C*, Immunostaining for BDNF in the adult mouse RMS. Inset shows colocalization of BDNF (green) and GFAP (red). Scale bar, 10  $\mu$ m. *D*, Immunostaining for BDNF (green) and GFAP (red) in the adult mouse RMS after osmotic minipump infusion of TrkB-Fc or IgG-Fc, as a control. BDNF immunostaining is drastically reduced after 7 d of TrkB-Fc infusion. Scale bar, 10  $\mu$ m. *E*, Coculture of astrocytes with BDNF-GFP-transfected endothelial cells. Note the strong GFP signal in the endothelial cells and punctate staining (arrows) of astrocyte. Bright-field (BF) images are also shown. Bleaching area is indicated by the red square. After 8 min of recovery period, the punctate staining reappears at the surface of astrocyte. Scale bar, 10  $\mu$ m.

intensity of immunostaining for this trophic factor on astrocytes ( $n = 4$  animals) (Fig. 3*D*). In addition, coculturing of SVZ astrocytes with BDNF-GFP-transfected endothelial cells revealed punctate staining for GFP on the surface of these glial cells (Fig. 3*E*). This punctate labeling reappears several minutes after bleaching of GFP on the astrocytes ( $n = 10$  cells from 3 independent experiments) (Fig. 3*E*). No such staining was observed in control experiments when astrocytes were cocultures with only

GFP-transfected endothelial cells (data not shown). These data suggest that BDNF is synthesized by the endothelial cells, secreted into the extracellular space, and bound to receptors on astrocytic processes. Importantly, the pattern of BDNF expression was not observed outside of the RMS, in which neuroblast migration ends (granule cell layer of the OB) or is not observed (striatum) (supplemental Figs. 1, 2, available at [www.jneurosci.org](http://www.jneurosci.org) as supplemental material). Astrocytes were devoid of BDNF immunoreac-

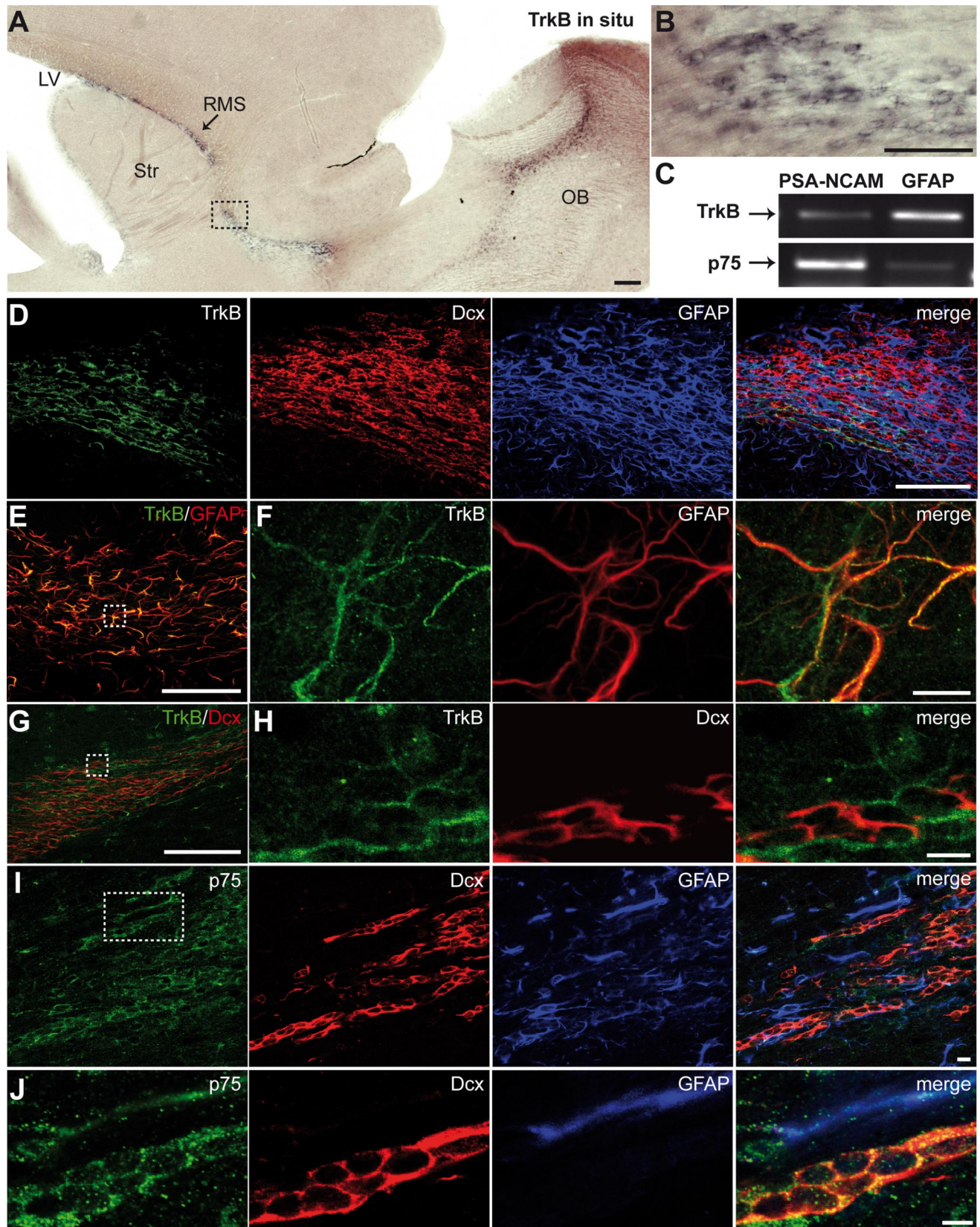


**Figure 4.** Expression of TrkB and p75NTR in the adult RMS. *A*, *In situ* hybridization for TrkB in the adult SVZ–OB pathway. Note the intense labeling in the adult RMS. Scale bar, 100  $\mu$ m. LV, Lateral ventricle; Str, striatum. *B*, High-magnification images of the boxed areas in *A*. Scale bar, 10  $\mu$ m. *C*, RT-PCR analysis of FACS-purified astrocytes (GFAP) and neuroblasts (PSA-NCAM). Note the high level of expression of p75NTR in neuroblasts and TrkB receptors in astrocytes. *D*, Immunostaining for TrkB (green), Dcx (red), and GFAP (blue) in the adult mouse RMS. Scale bar, 100  $\mu$ m. *E*, *F*, Immunostaining for TrkB (green) and GFAP (red) in the adult mouse RMS. *F*, High-magnification images of the boxed area in *E*. Scale bars: *E*, 100  $\mu$ m; *F*, 10  $\mu$ m. *G*, *H*, Micrographs showing that most, if not all, of TrkB (green) immunopositivity is not localized in Dcx-immunopositive cells (red). *H*, High-magnification images of the boxed area in *G*. Scale bars: *G*, 100  $\mu$ m; *H*, 10  $\mu$ m. *I*, *J*, Micrographs displaying expression of p75NTR (green) by migrating neuroblasts (Dcx, red). *J*, High-magnification images of the boxed area in (*I*). Scale bar, 10  $\mu$ m.

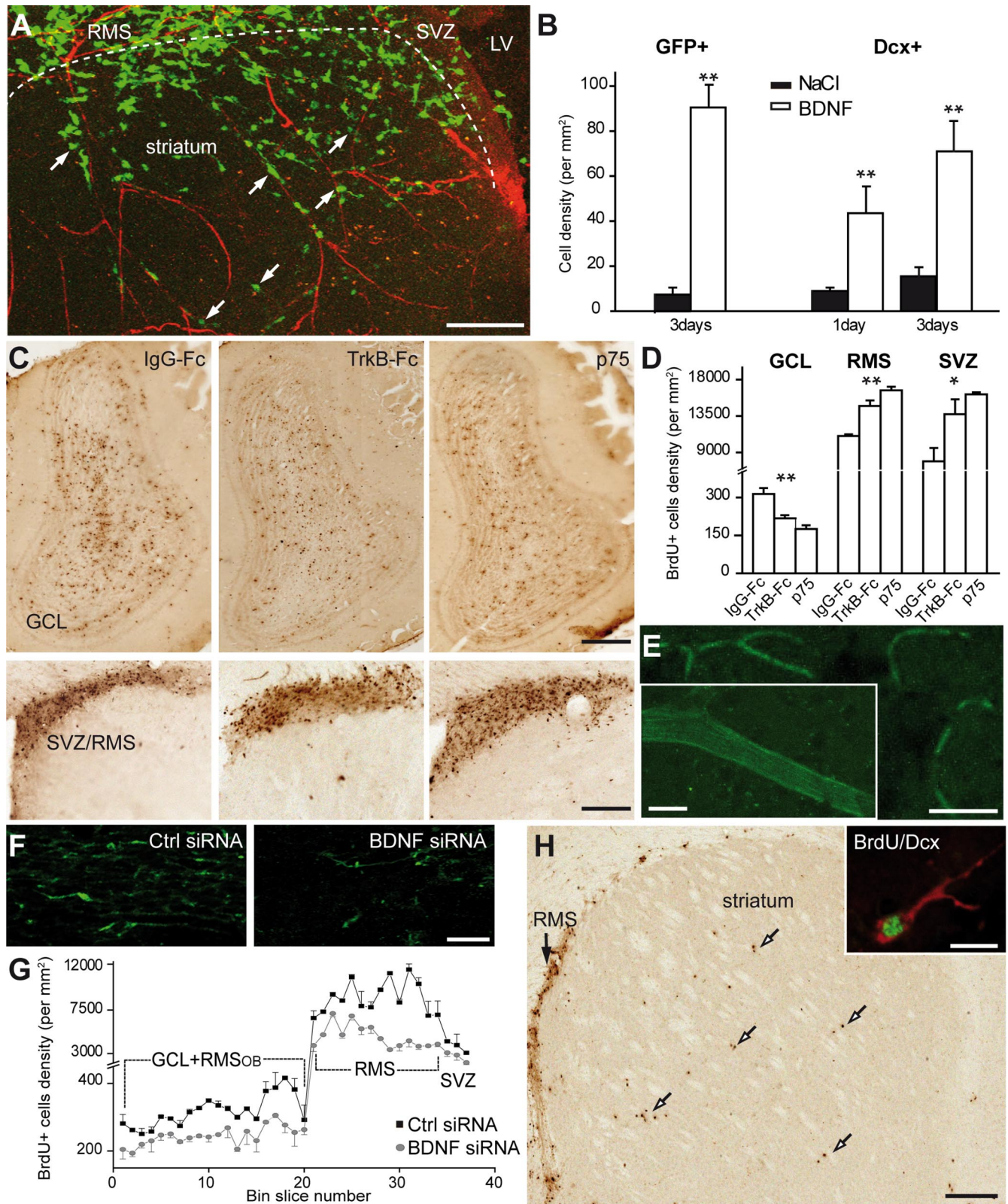


**Figure 5.** BDNF induces vasculature-associated cell migration in the adult forebrain. **A**, Micrographs illustrating migration of GFP<sup>+</sup> neuroblasts into the striatum 3 d after stereotaxic injection of BDNF (100 ng) to this region. GFP-expressing retrovirus was injected into the SVZ 2 d before injection of BDNF. Note that numerous migrating neuroblasts (arrows) use blood vessels for their navigation into the striatum. LV, Lateral ventricle. Scale bar, 100  $\mu$ m. **B**, Quantification of the density of GFP<sup>+</sup> and Dcx<sup>+</sup> derouted cells in the striatum. **C**, Micrographs showing BrdU<sup>+</sup> cells in the OB and SVZ/RMS 7 d after osmotic minipump infusions of IgG-Fc (10–90  $\mu$ g/ml), TrkB-Fc (10  $\mu$ g/ml), and p75NTR function-blocking antibodies (90  $\mu$ g/ml) just above horizontal limb of the RMS. BrdU was injected 2 d before osmotic minipump installation. Note the reduced number of BrdU<sup>+</sup> cells in the OB and increased number in the SVZ/RMS of TrkB-Fc and p75NTR function-blocking antibody infused animals. Scale bar, 100  $\mu$ m. **D**, Density of BrdU<sup>+</sup> cells in the granule cell layer (GCL) of the OB, RMS, and SVZ of IgG-Fc, TrkB-Fc, and p75NTR function-blocking antibody infused animals. **E**, Labeling of blood vessels after osmotic minipump infusion of fluorescently tagged BDNF siRNA to the carotid artery. Control and BDNF siRNAs were infused for 7 d. Inset shows high-magnification image of fluorescently tagged siRNA-labeled blood vessel. Scale bars: **E**, 50  $\mu$ m; inset, 10  $\mu$ m. **F**, Immunostaining for BDNF in the control and BDNF (Figure legend continues.)

tivity in these regions (supplemental Fig. 2, available at [www.jneurosci.org](http://www.jneurosci.org) as supplemental material).

We next performed immunostaining, *in situ* hybridization, and semiquantitative RT-PCR on FACS-purified neuroblasts and on astrocytes to determine which cell types in the adult RMS expressed the neurotrophin receptors TrkB and p75NTR. TrkB was found mostly on astrocytes (Fig. 4A–H), whereas p75NTR was expressed mainly by migrating neuroblasts (Fig. 4C, I, J) and by a small fraction of GFAP-immunopositive cells (Fig. 4J). In the adult SVZ, p75NTR immunoreactivity was also observed in C-type cells (Young et al., 2007). Evaluation of FACS-purified p75NTR<sup>+</sup> population of cells in the SVZ revealed that 20.2 ± 1.3% of cells were neurosphere-forming cells ( $n = 3$  independent sorting experiments), as reported previously (Young et al., 2007). However, already in the SVZ, ~38 and 7% of FACS-isolated p75NTR<sup>+</sup> cells were Dcx<sup>+</sup> and GFAP<sup>+</sup>, respectively ( $n = 3$  independent sorting experiments). These data indicate that p75NTR starts to be expressed by some migrating neuroblasts in the SVZ. We were not able to detect C-type cells expressing p75NTR immunoreactivity in the RMS, in contrast to what was reported recently (Bath et al., 2008). It has been shown previously that this population of cells is virtually absent in the adult RMS (Jankovski and Sotelo, 1996; Lois et al., 1996; Doetsch et al., 1997; Gritti et al., 2002).

### BDNF fosters neuronal migration via p75NTR

The expression patterns of BDNF and its receptors suggest that this trophic factor might be involved in the vasculature-associated migration of neuronal precursors. To investigate the role of BDNF in the neuronal migration in adult brain, we delivered this trophic factor into the striatum, a brain region that borders the migrating stream but in which neuronal precursors do not normally migrate. Three days after stereotaxic injection of BDNF (100 ng) in the striatum, numerous GFP<sup>+</sup> neuronal precursors (stereotaxically labeled in the SVZ with a retroviral vector encoding GFP 2 d before application of BDNF) were derouted from their normal migratory pathway toward the BDNF-injected zone, whereas few were derouted after a control saline injection (8.2 ± 1.4 cells/mm<sup>2</sup> in control vs 90.1 ± 12.4 cells/mm<sup>2</sup> in BDNF-injected mice;  $n = 3$  animals;  $p < 0.001$ ) (Fig. 5A, B). Remarkably, 75.0 ± 3.6 of these derouted cells still migrated along blood vessels ( $n = 3$  animals) (Fig. 5A). Similarly, the density of Dcx<sup>+</sup> precursors was increased in the striatum 1 and 3 d after BDNF injection (9.4 ± 1.1 cells/mm<sup>2</sup> in control vs 43.5 ± 16.0 cells/mm<sup>2</sup> in 1 d BDNF-injected mice,  $n = 3$  animals,  $p < 0.001$ ; and 12.6 ± 4.1 cells/mm<sup>2</sup> in control vs 71.2 ± 13.0 cells/mm<sup>2</sup> in 3 d BDNF-injected mice,  $p < 0.001$ ;  $n = 3$  animals per group) (Fig. 5B) (supplemental Fig. 3, available at [www.jneurosci.org](http://www.jneurosci.org) as supplemental material). To remove endogenous BDNF from the RMS, we implanted osmotic minipumps containing either TrkB-Fc or IgG-Fc (10 μg/ml) just above the horizontal limb of the RMS. After 7 d treatment, BrdU<sup>+</sup> cells, with BrdU being injected 2 d before installation of pumps, were sharply reduced in the OB of TrkB-Fc-treated

animals (313.5 ± 23.3 cells/mm<sup>2</sup> in IgG-Fc vs 216.8 ± 13.1 cells/mm<sup>2</sup> in TrkB-Fc-infused mice;  $n = 4$  animals;  $p < 0.001$ ) (Fig. 5C, D). Interestingly, this reduction in the OB was accompanied by concomitant increase in BrdU<sup>+</sup> cells in the RMS and SVZ (11,021.5 ± 221.4 cells/mm<sup>2</sup> in IgG-Fc vs 14,733.0 ± 698.7 cells/mm<sup>2</sup> in TrkB-Fc-infused mice for the RMS,  $p < 0.001$ ; and 8212.0 ± 1631.7 cells/mm<sup>2</sup> in IgG-Fc vs 13,736.2 ± 1836.8 cells/mm<sup>2</sup> in TrkB-Fc-infused mice for the SVZ,  $n = 4$  animals,  $p < 0.05$ ) (Fig. 5C, D). Similar results were obtained when the Dcx immunofluorescence intensity was analyzed in the OB of TrkB-Fc-infused animals (supplemental Fig. 3, available at [www.jneurosci.org](http://www.jneurosci.org) as supplemental material). Cell survival in the RMS was not affected by TrkB-Fc infusion (supplemental Fig. 3, available at [www.jneurosci.org](http://www.jneurosci.org) as supplemental material). Thus, our *in vivo* gain-of-function and loss-of-function experiments demonstrates that BDNF plays a crucial role in neuronal migration in the adult brain and are compatible with recent observations of decreased number of BrdU<sup>+</sup> cells in the OB of BDNF haploinsufficient mice 28 d after BrdU injection (Bath et al., 2008).

Because migrating neuroblasts express p75NTR, we investigated whether this receptor is involved in BDNF-induced migration. For this, we implanted osmotic minipumps containing either function-blocking antibodies for p75NTR (Clary and Reichardt, 1994) or IgG-Fc (90 μg/ml) just above the horizontal limb of the RMS. This treatment reduced the number of Dcx<sup>+</sup> (supplemental Fig. 3, available at [www.jneurosci.org](http://www.jneurosci.org) as supplemental material) and BrdU<sup>+</sup> cells in the OB (313.5 ± 23.3 cells/mm<sup>2</sup> in IgG-Fc vs 175.0 ± 14.7 cells/mm<sup>2</sup> in p75NTR-antibody-infused mice;  $n = 3$  animals;  $p < 0.001$ ) (Fig. 5C, D) and increased their number in the RMS and SVZ (11,021.5 ± 221.4 cells/mm<sup>2</sup> in IgG-Fc vs 16,920.0 ± 444.9 cells/mm<sup>2</sup> in p75NTR-antibody-infused mice for the RMS; and 8212.0 ± 1631.7 cells/mm<sup>2</sup> in IgG-Fc vs 16,177.2 ± 254.4 cells/mm<sup>2</sup> in p75NTR-antibody-infused mice for the SVZ;  $n = 3$  animals;  $p < 0.001$ ) (Fig. 5C, D). These results demonstrate that BDNF-p75NTR interaction is important for the accumulation of neuronal precursors in the adult OB.

Recent studies have shown that TrkB haploinsufficient mice have a reduced number of BrdU<sup>+</sup> cells in the OB 28 d after BrdU injection (Bath et al., 2008). Whereas TrkB receptors are mostly found on astrocytes (Fig. 4C–G), low level of their expression is also detected in neuroblasts (Fig. 4C), and, from these experiments, it was not clear whether the reduced number of BrdU<sup>+</sup> cells in the OB results from the alterations of TrkB expression on astrocytes or neuroblasts. To address this issue, we analyzed the number of BrdU<sup>+</sup> cells in the RMS<sub>OB</sub> of mice lacking TrkB expression in astrocytes. To produce these animals, we crossed animals bearing a floxed TrkB allele (Minichiello et al., 1999) with *GlastCre::ERT2* mice (Mori et al., 2006), which carry tamoxifen-inducible form of Cre in the *GLAST* locus. Because neuronal precursors are derived from GFAP-expressing cells (Alvarez-Buylla and Garcia-Verdugo, 2002; Lledo and Saghatelian, 2005) and, therefore, can be also affected in these transgenic animals, we performed all our analysis 5 d after the end of tamoxifen treatment. At this stage, only 4 ± 2% of recombined neuroblasts (assessed by the Dcx immunoreactivity and the presence of the reporter protein in *GlastCre::ERT2/ZEG* mice) were present in the RMS<sub>OB</sub>. In contrast, 69.6 ± 8.8% of astrocytes were found to be recombined in the RMS, as it has been reported for the adult SVZ (Mori et al., 2006). Five days after BrdU injection, with BrdU being injected at the end of tamoxifen treatment, the number of BrdU<sup>+</sup> cells was drastically reduced in the RMS<sub>OB</sub> of TrkB<sup>fl/fl</sup> *GLAST::CreERT2* mice compared with the control TrkB<sup>wildtype/wildtype</sup>

←  
(Figure legend continued.) siRNAs-treated animals. Note the reduced intensity of immunostaining. Scale bar, 20 μm. **G**, Density of BrdU<sup>+</sup> cells in the SVZ–OB pathway after control (black squares) and BDNF (gray squares) siRNA infusion to the carotid artery. Single pulse of BrdU was given 6 h before installation of osmotic minipumps. BrdU<sup>+</sup> cells were counted in the coronal sections spaced by 120 μm throughout the SVZ–OB pathway. **H**, Micrographs displaying BrdU<sup>+</sup> cells in the RMS of BDNF siRNA-treated animals. Note that numerous BrdU<sup>+</sup> cells (arrows) leave RMS and migrate to the striatum. Inset shows high-magnification image of BrdU (green) and Dcx (red) colabeled cell in the striatum. Scale bars: **H**, 100 μm; inset, 10 μm.

GLAST::CreERT2 animals ( $10,642.2 \pm 187.9$  cells/mm<sup>2</sup> in wild-type vs  $6560.0 \pm 89.7$  cells/mm<sup>2</sup> in TrkB<sup>fl/fl</sup> GLAST::CreERT2 mice;  $n = 4$  animals;  $p < 0.001$ ) (supplemental Fig. 4, available at www.jneurosci.org as supplemental material). Because (1) this 40% reduction in the number of BrdU<sup>+</sup> cells cannot be explained by the 4% of recombined neuroblasts in the RMS<sub>OB</sub> and (2) cell proliferation and survival analyzed immediately after the end of tamoxifen treatment were not affected in the RMS and SVZ (data now shown), we conclude that TrkB receptors expressed on astrocytes play an important role in neuroblast migration in the RMS.

Our data show that application of TrkB-Fc reduced the number of BrdU<sup>+</sup> cells in the OB (Fig. 5C,D) and that endothelial cells are a likely candidate for the source of BDNF in the RMS (Fig. 3A,B). To directly show that blood vessel-derived BDNF is involved in the arrival of newborn cells, we next attempted to downregulate its expression specifically in the blood vessels and only in adults. For this, we inserted a catheter connected to the 7 d osmotic minipump to the external carotid artery. Figure 5E shows that, with this approach, fluorescently tagged BDNF siRNAs accumulate in blood vessels but not in other cell types of the adult brain. Importantly, infusion of BDNF siRNA reduces the expression of BDNF in the adult RMS by  $38.45 \pm 10.6\%$  (data were normalized for GFAP immunostaining;  $n = 3$  animals) (Fig. 5F) that consequently decreased the number of BrdU<sup>+</sup> cells all along the SVZ–OB pathway ( $n = 3$  animals;  $p < 0.001$ ) (Fig. 5G). Although these data do not exclude possibility that endothelial cell-derived BDNF has also a nonmigratory role (such as cell proliferation, survival, and differentiation), the reduction in the BrdU<sup>+</sup> cells in the adult SVZ–OB was at least partially attributable to the immigration of these cells to neighboring territories, such as striatum ( $0.5 \pm 0.3$  cells/mm<sup>2</sup> in control vs  $30.2 \pm 8.9$  cells/mm<sup>2</sup> in BDNF siRNA-treated animals) (Fig. 5H).

Altogether our *in vivo* experiments demonstrate that BDNF is important for the proper navigation of neuronal precursors in the adult brain and that p75NTR as well as TrkB receptors expressed on the astrocytes are involved in this process. However, the physiological mechanisms that govern neuronal migration are very complex (Fig. 2C–F), and, from our *in vivo* experiments, it is difficult to discern the direct and acute role of BDNF, TrkB, or p75NTR. We therefore directly tested whether BDNF, TrkB, and p75NTR affect neuronal migration, using time-lapse video microscopy in the acute slices of the adult mouse forebrain. Bath application of BDNF (10 ng/ml) increased the average distance covered by migrating cells, the number of cells in the migratory phase, and decreased the duration of the resting period (Fig. 6A–C) (Table 1) (supplemental Video 5, available at www.jneurosci.org as supplemental material). In contrast, application of TrkB-Fc (1 μg/ml) decreased the average distance covered by migrating cells, decreased the number of cells in the migratory phase, and increased the duration of the stationary period (Fig. 6C) (see also Fig. 7B; Table 1) (supplemental Video 6, available at www.jneurosci.org as supplemental material). Application of TrkB-Fc together with BDNF either slightly increased or decreased or had no effect on the migratory behavior of neuroblasts depending on the concentration of BDNF (supplemental Fig. 5, available at www.jneurosci.org as supplemental material). In agreement with our *in vivo* experiments with function-blocking antibodies for p75NTR, incubation of acute adult mouse forebrain slices in these antibodies (20 μg/ml) drastically reduced the average distance that cells migrated, decreased the number of cells in the migratory phase, and increased the duration of the stationary period (Fig. 6D–F; Table 1). Importantly, investigation of neuronal migration in the acute slices prepared from

p75NTR-deficient animals revealed very similar defects in migration (Fig. 6F–I; Table 1) (supplemental Video 7, available at www.jneurosci.org as supplemental material). The average distance that cells migrated as well as the number of cells in the migratory phase were drastically reduced, whereas the duration of the stationary period was increased. Moreover, bath application of BDNF (10 ng/ml), TrkB-Fc (1 μg/ml), or p75NTR function-blocking antibodies did not affect the migratory behavior of neuroblasts in the acute slices prepared from p75NTR-deficient animals (Fig. 6G–I; Table 1) (supplemental Video 7, available at www.jneurosci.org as supplemental material). These experiments suggest that p75NTR, but not TrkB receptors, expressed by neuroblasts control their migratory behavior. In agreement with these results are our observations showing that application of Trk inhibitor K252a (200 nM) did not affect the migration of neuronal precursors in the wild-type animals (Table 1) (supplemental Fig. 6, available at www.jneurosci.org as supplemental material). Despite the reductions in net migration observed, migration velocity was not altered after incubation of slices with p75NTR function-blocking antibodies, after application of BDNF and TrkB-Fc, or in p75NTR-deficient animals (data not shown).

Finally, we tested vasculature-associated neuroblasts migration *in vitro*, in a tissue-engineered 3D connective tissue made of fibroblasts and endothelial cells, in which a network of BDNF-expressing capillary-like tubes mimicking blood capillaries, is formed (Berthod et al., 2006) (Fig. 6J). Coculturing of GFP<sup>+</sup> neuroblasts with reconstituted capillaries showed that most of the migrating cells ( $78.6 \pm 6.9\%$ ;  $n = 52$  cells of 3 cultures) accumulate along the BDNF-expressing vessels (Fig. 6K,L). Time-lapse video imaging of cell migration in culture revealed a twofold increase in the distance of migration for the neuroblasts located close to the capillaries compared with those cocultured with fibroblasts alone ( $0.12 \pm 0.01$  μm/15 s in capillary culture,  $n = 41$  cells of 4 cultures vs  $0.05 \pm 0.01$  μm/15 s in fibroblasts cultures,  $n = 15$  cells of 3 cultures;  $p < 0.001$ ) (Fig. 6M). Reducing BDNF expression in the endothelial cells of capillaries by siRNA (Fig. 6M, inset) strongly reduced the proportion of capillary-associated migrating cells ( $57.9 \pm 8.1\%$ ;  $n = 32$  cells of 3 cultures) and the mean distance that neuroblasts propagate ( $0.12 \pm 0.01$  μm/15 s in control siRNA,  $n = 12$  cells of 3 cultures vs  $0.08 \pm 0.01$  μm/15 s in BDNF siRNA,  $n = 15$  cells of 3 cultures;  $p < 0.001$ ) (Fig. 6M). Blocking p75NTR receptors on neuroblasts with function-blocking antibodies also decreased the migration of neuronal precursors ( $0.12 \pm 0.01$  μm/15 s in IgG-Fc,  $n = 10$  cells of 3 cultures vs  $0.08 \pm 0.01$  μm/15 s in p75NTR function-blocking antibodies,  $n = 16$  cells of 3 cultures;  $p < 0.001$ ) (Fig. 6M).

Altogether, our *in vitro* data in the acute slices of the adult mouse forebrain as well as in the tissue-engineered capillaries clearly demonstrate that BDNF fosters neuronal migration in a p75NTR-dependent manner. But what is the role of astrocytes in the vasculature-associated neuroblasts migration, why BDNF is trapped by the RMS astrocytes, and why did conditional removal of TrkB in the astrocytes reduce the number of BrdU<sup>+</sup> cells in the OB?

#### Role of astrocytes in the vasculature-associated migration of the adult neuronal precursors

BDNF secretion is a Ca<sup>2+</sup>-dependent process (Goggi et al., 2003), and, in some brain regions, BDNF bound to cell-surface TrkB receptors on astrocytes can be released into extracellular environment (Rubio, 1997; Alderson et al., 2000). It is, thus, conceivable

**Table 1. Migration of neuronal precursors and Ca<sup>2+</sup> fluctuations in astrocytes in the acute slices of the adult mouse forebrain**

Experiment		Distance of migration ( $\mu\text{m}$ )	Cells in the migratory phase (%)	Duration of the resting period (s)	Rate of migration ( $\mu\text{m}/\text{h}$ )	Frequency of Ca <sup>2+</sup> fluctuations (peak/min)	Number of cells/slices/animals
Migration in the RMS control		0.32 $\pm$ 0.02	47.4 $\pm$ 2.0	492.3 $\pm$ 41.5	121.2 $\pm$ 3.9		64/14/10
Application of BDNF (10 ng/ml)	Ctrl	0.34 $\pm$ 0.01	44.9 $\pm$ 2.0	274.2 $\pm$ 13.8	136.4 $\pm$ 5.2		376/4/4
	BDNF	0.43 $\pm$ 0.02*	57.4 $\pm$ 1.2*	147.5 $\pm$ 5.6*	142.6 $\pm$ 6.9		
Application of TrkB-Fc (1 $\mu\text{g}/\text{ml}$ )	IgG-Fc	0.33 $\pm$ 0.02	49.4 $\pm$ 2.1	260.5 $\pm$ 12.7	115.7 $\pm$ 7.3		162/4/4
	TrkB-Fc	0.16 $\pm$ 0.04*	24.3 $\pm$ 6.2*	713.2 $\pm$ 160.0*	88.3 $\pm$ 8.8		194/4/4
Application of p75NTR (20 $\mu\text{g}/\text{ml}$ )	IgG-Fc	0.33 $\pm$ 0.03	47.0 $\pm$ 3.3	243.6 $\pm$ 28.1	121.1 $\pm$ 6.7		91/4/4
	p75NTR	0.16 $\pm$ 0.01*	24.6 $\pm$ 1.1*	558.7 $\pm$ 2.9**	101.5 $\pm$ 6.6		138/5/3
Application of K252a (200 nM)	Ctrl	0.33 $\pm$ 0.05	48.3 $\pm$ 7.9	293.5 $\pm$ 44.2	135.3 $\pm$ 4.1		125/2/2
	K252a	0.30 $\pm$ 0.06	44.4 $\pm$ 6.9	294.5 $\pm$ 55.9	127.1 $\pm$ 1.9		
p75NTR-WT		0.33 $\pm$ 0.01	47.1 $\pm$ 1.4	259.4 $\pm$ 10.9	124.4 $\pm$ 4.3		150/5/4
p75NTR-KO		0.18 $\pm$ 0.03*	26.9 $\pm$ 4.2**	735.1 $\pm$ 101.1**	121.7 $\pm$ 8.4		200/6/6
Application of BDNF (10 ng/ml) in p75NTR-KO	Ctrl	0.19 $\pm$ 0.06	25.2 $\pm$ 6.4	750.5 $\pm$ 158.4	121.7 $\pm$ 13.3		168/4/4
	BDNF	0.2 $\pm$ 0.06	26.2 $\pm$ 7.1	760.0 $\pm$ 156.3	125.9 $\pm$ 10.3		
Application of TrkB-Fc (1 $\mu\text{g}/\text{ml}$ ) in p75NTR-KO	Ctrl	0.18 $\pm$ 0.06	30.1 $\pm$ 1.9	704.2 $\pm$ 38.4	121.6 $\pm$ 2.7		88/2/2
	TrkB-Fc	0.18 $\pm$ 0.02	28.8 $\pm$ 2.1	721.8 $\pm$ 21.1	122.4 $\pm$ 11.4		
Ca <sup>2+</sup> activity in the RMS control						0.49 $\pm$ 0.0004	125/27/10
Application of GABA (10 $\mu\text{M}$ )	Ctrl	0.41 $\pm$ 0.04	55.7 $\pm$ 2.9	262.0 $\pm$ 33.7	110.8 $\pm$ 10.6	0.42 $\pm$ 0.001	27/4/3 for Ca <sup>2+</sup> activity
	GABA	0.17 $\pm$ 0.04**	28.1 $\pm$ 5.1*	584.6 $\pm$ 16.1**	79.8 $\pm$ 7.9*	0.58 $\pm$ 0.001**	146/5/5 for migration
Application of bicuculline methochloride (100 $\mu\text{M}$ )	Ctrl	0.24 $\pm$ 0.01	40.6 $\pm$ 1.8	255.0 $\pm$ 27.3	93.8 $\pm$ 3.9	0.52 $\pm$ 0.0007	53/7/5 for Ca <sup>2+</sup> activity
	Bic	0.35 $\pm$ 0.03*	51.5 $\pm$ 2.8*	168.0 $\pm$ 17.7*	135.3 $\pm$ 6.9*	0.32 $\pm$ 0.001*	130/7/5 for migration
Application of TrkB-Fc (1 $\mu\text{g}/\text{ml}$ )–TrkB-Fc (1 $\mu\text{g}/\text{ml}$ )	TrkB-Fc	0.19 $\pm$ 0.04	28.5 $\pm$ 5.8	814.0 $\pm$ 79.0	109.1 $\pm$ 2.5		67/2/2
Application of TrkB-Fc (1 $\mu\text{g}/\text{ml}$ )–GABA (10 $\mu\text{M}$ )	GABA	0.16 $\pm$ 0.06	25.5 $\pm$ 9.0	864.5 $\pm$ 281.0	114.3 $\pm$ 4.5		105/2/2
Application of GABA (10 $\mu\text{M}$ )–TrkB-Fc (1 $\mu\text{g}/\text{ml}$ )	GABA	0.14 $\pm$ 0.02	26.1 $\pm$ 4.7	704.6 $\pm$ 8.8	111.5 $\pm$ 11.6		71/2/2
	TrkB-Fc	0.11 $\pm$ 0.0001	19.9 $\pm$ 0.06	781.2 $\pm$ 9.8	109.1 $\pm$ 3.4		
Application of 2-APB (100 $\mu\text{M}$ )	Ctrl	0.32 $\pm$ 0.05	48.4 $\pm$ 0.3	276.5 $\pm$ 16.2	120.5 $\pm$ 2.8	0.46 $\pm$ 0.048	40/4/4 for Ca <sup>2+</sup> activity
	2-APB	0.01 $\pm$ 0.001**	1.1 $\pm$ 1.1*	738.0 $\pm$ 37.9	87.5 $\pm$ 0.3*	0.08 $\pm$ 0.025***	45/2/2 for migration

Bic, Bicuculline; Ctrl, control; KO, knock out; WT, wild type.

that, in the RMS, Ca<sup>2+</sup> activity in astrocytes may induce secretion of BDNF or release BDNF from cell-surface TrkB receptors. Ca<sup>2+</sup> activity has also been implicated in the trafficking of TrkB to the plasma membrane (Du et al., 2003), and it is possible that Ca<sup>2+</sup> fluctuations in the astrocytes induce TrkB insertion at the cell surface and thereby restrict the amount of extracellular BDNF available to neuroblasts. These potential links between Ca<sup>2+</sup> activity and BDNF level led us to test whether adult RMS astrocytes display Ca<sup>2+</sup> fluctuations and, if so, whether they regulate BDNF level available to migrating neuroblasts.

We loaded acute slices of the adult mouse forebrain with membrane-permeable Ca<sup>2+</sup> indicator Fluo4-AM. This indicator specifically enters astrocytes, but not neuroblasts, as revealed by the fact that, during the entire recording time (sometimes >2 h), none of the GFAP-expressing (data not shown) Fluo4-AM-loaded cells had migrated. Our Ca<sup>2+</sup> imaging studies demonstrate that RMS astrocytes and their processes display spontaneous Ca<sup>2+</sup> fluctuations (Fig. 7A) (supplemental Videos 8, 9, available at www.jneurosci.org as supplemental material) with the mean frequency of 0.49  $\pm$  0.004 peaks/min ( $n$  = 125 cells from 10 animals). Having shown spontaneous Ca<sup>2+</sup> fluctuations in RMS astrocytes, we next asked, what triggers Ca<sup>2+</sup> activity in these glial cells? Because (1) GABA depolarizes astrocytes and

induces an increase in intracellular [Ca<sup>2+</sup>] (Fraser et al., 1995), (2) astrocytes in the SVZ and RMS express functional GABA<sub>A</sub> receptors (Liu et al., 2005), and (3) migrating neuroblasts release GABA (Bolteus and Bordey, 2004), we hypothesized that migrating neuroblasts themselves control Ca<sup>2+</sup> activity in the astrocytes via GABAergic signaling.

To investigate the role of GABA in the triggering of Ca<sup>2+</sup> activity in astrocytes, we applied GABA (10  $\mu\text{M}$ ) or the GABA<sub>A</sub> receptor antagonist bicuculline methochloride (100  $\mu\text{M}$ ) to Fluo4-AM-loaded adult mouse forebrain slices and then performed combined real-time video imaging of Ca<sup>2+</sup> fluctuations in astrocytes and neuroblasts migration. Application of GABA increased the frequency of Ca<sup>2+</sup> fluctuations in astrocytes (Table 1) (supplemental Video 8, available at www.jneurosci.org as supplemental material) and decreased the average distance that migrating cells propagated, reduced the number of cells in the migratory phase, and increased the duration of the stationary period (Table 1). In contrast, bicuculline application drastically reduced the frequency of Ca<sup>2+</sup> fluctuations in astrocytes (Fig. 7A; Table 1) (supplemental Video 9, available at www.jneurosci.org as supplemental material) and increased the migration of neuronal precursors (Table 1). The application of bicuculline not only increased the rate of migration of neuronal precursors by 44.6  $\pm$

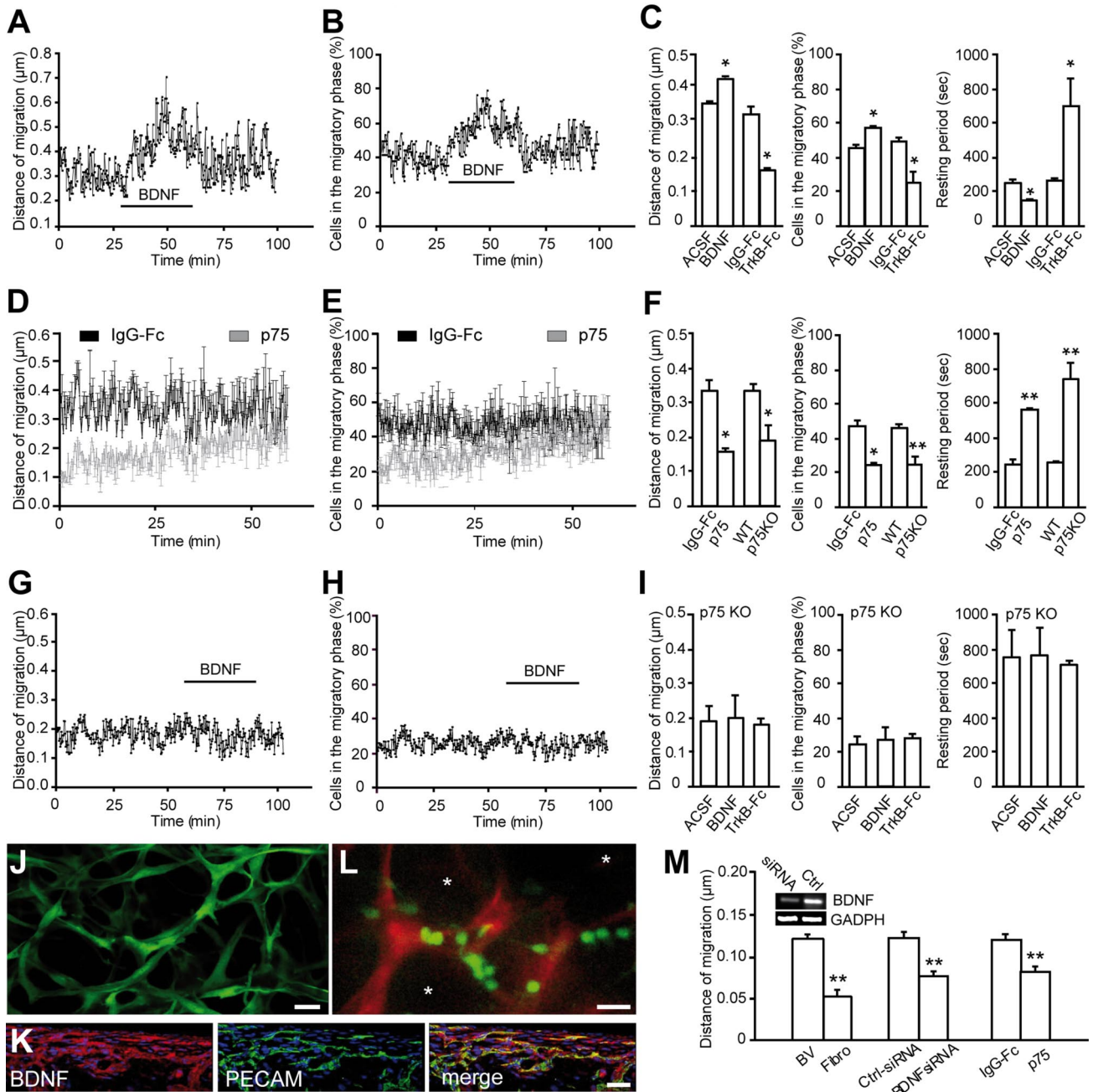


**Figure 6.** BDNF fosters neuronal migration via p75NTR. **A, B**, Individual experiment demonstrating that bath application of BDNF (10 ng/ml) increases the average distance that migrating cells propagate (**A**) and raises the percentage of cells that are in the migratory phase at each time point (**B**). The time period for BDNF application is shown by a black line. **C**, Summary graph showing the effect of BDNF or TrkB-Fc (1  $\mu\text{g}/\text{ml}$ ) applications on the average distance that migratory cells propagate (per 15 s), the percentage of cells in the migratory phase, and the duration of the stationary period. In control experiments, IgG-Fc (1  $\mu\text{g}/\text{ml}$ ) was applied instead of TrkB-Fc. **D, E**, Summary graphs showing that preincubation of slices with p75NTR function-blocking antibodies drastically decreases the average distance that migrating cells propagate (**D**) and reduces percentage of cells in the migratory phase at each time point (**E**). The time-lapse recording was performed after preincubation of slices in either p75NTR function-blocking antibodies or IgG-Fc (20  $\mu\text{g}/\text{ml}$ ) for 1 h. During the entire period of recording, the slices were continuously perfused with oxygenated ACSF (2 ml/min). Note that the blocking effect of p75NTR function-blocking antibodies is washed out during recording. **F**, Summary graph showing that deficiency in p75NTR and application of p75NTR function-blocking antibodies affects the average distance that migratory cells propagate (per 15 s), the percentage of cells in the migratory phase, and the duration of the stationary period. **G, H**, Individual experiment demonstrating that bath application of BDNF (10 ng/ml) does not affect the average distance that migrating cells propagate (**G**) and the percentage of cells in the migratory phase at each time point (**H**) in the slices prepared from p75NTR-deficient animals. **I**, Summary graph showing the absence of effect of BDNF and TrkB-Fc applications on the average distance that migratory cells propagate (per 15 s), the percentage of cells in the migratory phase, and the stationary period duration in p75NTR-deficient animals. **J**, Micrograph illustrating GFP<sup>+</sup> tissue-engineered 3D capillary-like network *in vitro*. Scale bar, 30  $\mu\text{m}$ . **K**, Immunostaining for BDNF (red) and PECAM (green) in the transversal sections of sponges containing capillary-like network. Scale bar, 50  $\mu\text{m}$ . **L**, Micrograph depicting GAD67-GFP<sup>+</sup> neuroblasts (green) cocultured in 3D capillary-like network (red). HUVEC cells were transfected with GFP lentivirus. GFP<sup>+</sup> neuroblasts (small cells of ~5–10  $\mu\text{m}$  size) and GFP<sup>+</sup> capillaries (long tubular-like structures) were easily distinguishable on the basis of their shapes and were false-colored in offline analysis using ImagePro software. Note that neuroblasts accumulate along the capillaries, and places that do not contain these capillary-like structures (asterisks) are also free of neuroblasts. Scale bar, 20  $\mu\text{m}$ . **M**, Quantification of neuroblast migration in the capillary-like network under different experimental conditions. Note the increased migration of neuronal precursors in the cultures containing capillary-like structure compared with the control fibroblast containing cultures (Fibro). Note also that BDNF siRNA and p75NTR function-blocking antibodies reduce the migration of neuronal precursors. Distance of migration (per 15 s) was calculated in the images acquired every 15 s for at least 1 h. Inset shows semiquantitative RT-PCR analysis of BDNF expression in the endothelial cells after siRNA transfection. KO, Knock-out; WT, wild type; BV, blood vessels.

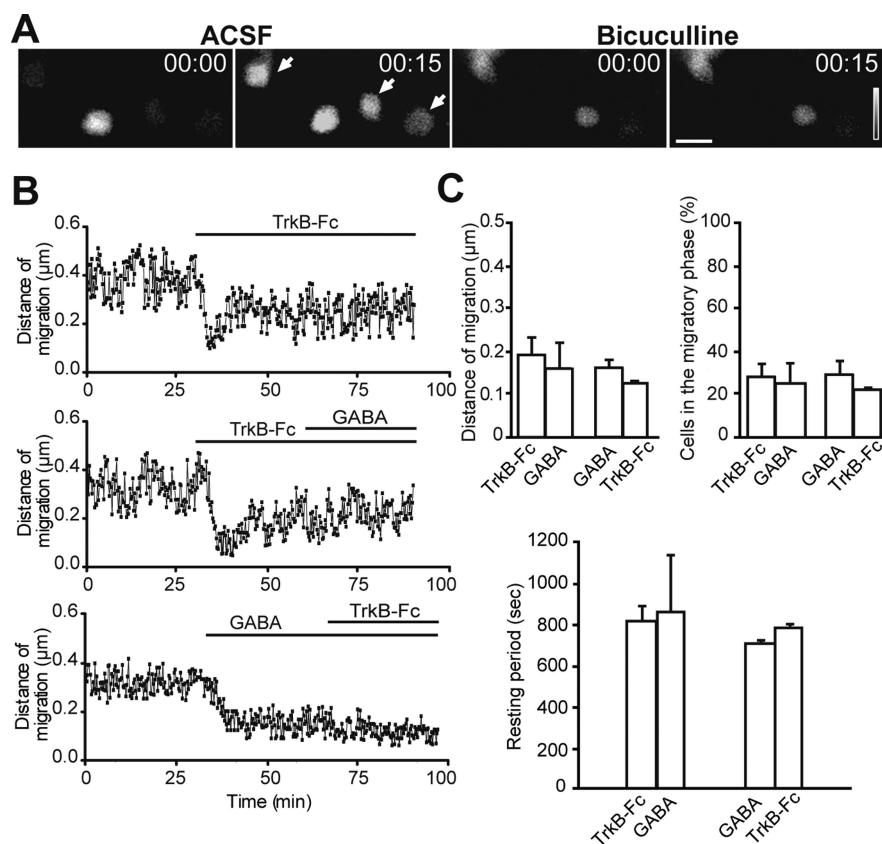


**Figure 7.** GABAergic signaling affects  $Ca^{2+}$  activity in astrocytes and migration of neuroblasts. **A**, Application of GABA<sub>A</sub> receptor antagonist bicuculline (Bic, 100 μM) diminishes spontaneous  $Ca^{2+}$  fluctuations in the astrocytes. Time-lapse video imaging illustrating changes in the fluorescent intensity under control conditions (left panels) and after application of bicuculline (right panels) over time (indicated in seconds in the top right corner of each photograph). Scale bar, 10 μm. **B**, Individual experiments demonstrating that both application of GABA (10 μM) after application of TrkB-Fc (1 μg/ml) as well as TrkB-Fc application after GABA application do not affect the average distance that migrating cells propagate. The time periods for TrkB-Fc and GABA applications are shown by black lines. Each time point represents the average value for 20–30 cells. **C**, Summary graphs illustrating that both application of GABA (10 μM) after application of TrkB-Fc (1 μg/ml) and bath application of TrkB-Fc (1 μg/ml) after application of GABA (10 μM) do not affect the average distance that migrating cells propagate (per 15 s), the percentage of cells in the migratory phase, and the duration of stationary period.

5.7% (Table 1), as reported previously (Bolteus and Bordey, 2004), but also significantly augmented the average distance that migrating cells propagated, increased the number of cells in the migratory phase and decreased the duration of the stationary period (Table 1). The  $Ca^{2+}$  fluctuations in astrocytes were most likely mediated by IP<sub>3</sub>-sensitive intracellular  $Ca^{2+}$  stores, because preapplication of 2-aminoethoxydiphenyl borate (2-APB) (100 μM) abolished the effect of bicuculline and GABA on the  $Ca^{2+}$  activity in astrocytes (supplemental Fig. 7, available at [www.jneurosci.org](http://www.jneurosci.org) as supplemental material). Thus, manipulation with GABAergic signaling in the adult RMS affects  $Ca^{2+}$  activity in the astrocytes and neuronal precursor migration in the manner that is reminiscent of the BDNF signaling manipulation. We, therefore, decided to investigate whether effect of GABA on the migration of neuronal precursors involves the BDNF pathway. For this, we first blocked BDNF pathway by application of TrkB-Fc (1 μg/ml) and then applied GABA (10 μM) (Fig. 7B). Under these conditions, GABA had no effect on the migratory behavior of neuroblasts (Fig. 7B,C; Table 1). Conversely, preapplication of GABA decreased the migration of neuronal precursors that was not possible to further reduce by application of TrkB-Fc (Fig. 7B,C; Table 1). These experiments suggest that BDNF and GABA control cell migration via the same pathway.

We then asked whether GABA-induced  $Ca^{2+}$  fluctuation in astrocytes might regulate local delivery of BDNF to neuroblasts. To address this, we prepared cultures of astrocytes from the adult SVZ. These cultures contain mostly astrocytes, as verified by the labeling for GFAP, Tuj1, and receptor-interacting protein, markers for astrocytes, neurons, and oligodendrocytes, respectively, and are immunopositive for TrkB (data not shown). To investigate whether  $Ca^{2+}$  activity in astrocytes induces BDNF release, we first preincubated these cultures with BDNF (10 ng/ml), washed extensively, and then treated with 10 μM GABA for 30 min. Activation of GABA<sub>A</sub> receptors on astrocytes did not change the amount of secreted BDNF in these cultures ( $92.7 \pm 5.9\%$  of control;  $n = 3$ ), indicating that GABA does not induce release of BDNF from astrocytes.

We then tested whether GABA-induced  $Ca^{2+}$  fluctuation in astrocytes might regulate trafficking of TrkB receptors and thereby control the amount of extracellular BDNF available to neuroblasts. We incubated acute adult mouse forebrain slices with bicuculline (100 μM) or GABA (10 μM) for 1 h, extracted the RMS, and analyzed surface TrkB receptor level by cell-surface biotinylation of the dissociated cells. Incubation of slices with bicuculline reduced the amount of TrkB receptors located at the surface of RMS cells to  $77.4 \pm 2.5\%$  of control levels ( $n = 4$  animals;  $p < 0.05$ ) (Fig. 8A), whereas treatment with GABA (10 μM) increased their amount to  $122.4 \pm 5.1\%$  ( $n = 4$  animals;  $p < 0.05$ ) (Fig. 8A). Interestingly, blocking  $Ca^{2+}$  fluctuations in astrocytes by 2-APB

(100 μM) reduced the amount of TrkB receptors located at the surface to  $63.2 \pm 10.1\%$  ( $n = 3$  animals;  $p < 0.05$ ) (Fig. 8A). It is also noteworthy that incubation of slices with BDNF (10 ng/ml) for 1 h decreased the amount of surface TrkB receptors to  $77.9 \pm 6.5\%$  ( $n = 3$  animals;  $p < 0.05$ ) (Fig. 8A).

These data suggest that modulation of  $Ca^{2+}$  fluctuations in astrocytes by endogenous GABAergic signaling is required for plasma membrane insertion of TrkB receptors and that binding of BDNF to this receptor induces its internalization. If endogenous GABAergic signaling induces the insertion of TrkB receptors on the plasma membrane, then blocking GABA<sub>A</sub> receptors with bicuculline should decrease trapping of BDNF by astrocytes. Indeed, BDNF immunostaining in slices previously incubated with bicuculline (100 μM) for 1 h induced a twofold reduction in BDNF labeling ( $51.05 \pm 0.4\%$  decrease; data were normalized for GFAP immunostaining;  $n = 3$  animals) (Fig. 8B). These results suggest that GABAergic signaling from neuroblasts facilitates insertion of TrkB on the plasma membrane of RMS astrocytes. The newly inserted TrkB receptor is then able to bind to BDNF and therefore might act to reduce BDNF availability for migrating neuronal precursors. Through this pathway, neuroblasts might control the periodicity of their migratory and stationary phases and thus their own migration.

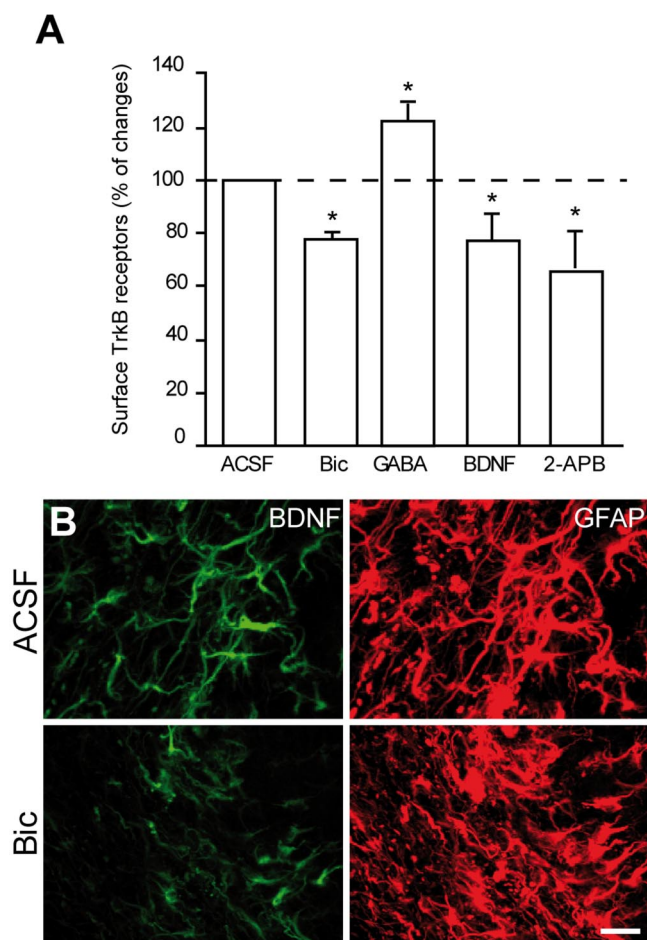


**Figure 8.** GABA induces insertion of TrkB receptors on membrane of astrocytes. **A**, Preincubation of slices with bicuculline (Bic; 100  $\mu$ M), BDNF (10 ng/ml), or 2-APB (100  $\mu$ M) for 1 h reduces amount of surface TrkB receptors. In contrast, treatment with GABA (10  $\mu$ M for 1 h) increases the amount of surface TrkB receptors. The cell-surface molecules of freshly isolated cells, extracted from RMS, were labeled with Sulfo-NHS-biotin. Cell lysates were precipitated with streptavidin-coated agarose beads and immunolabeled with TrkB antibodies. The amount of surface TrkB receptors was analyzed by ELISA. **B**, Incubation of acute slices of the adult mouse forebrain with bicuculline (100  $\mu$ M) decreases immunolabeling for BDNF in the adult RMS. Scale bar, 10  $\mu$ m.

## Discussion

The present study has demonstrated that blood vessels provide structural organization and molecular cues important for neuroblast migration in the adult brain. Our data reveal that vasculature parallels the migratory stream of neuronal precursors and guides them toward and into OB. We also discovered the underlying mechanism of vasculature-associated migration of neuronal precursors. Our data suggest that the endothelial cells of blood vessels constitutively synthesize BDNF, which is released within the extracellular space and fosters neuronal migration via p75NTR expressed by these migrating cells. We hypothesize that migrating neuroblasts control their own migration by regulating the amount of free extracellular BDNF. GABA released from neuronal precursors induces  $Ca^{2+}$ -dependent insertion of high-affinity TrkB receptors into the plasma membrane of astrocytes that ensheath migrating neuroblasts and contact blood vessels. This leads to trapping of extracellular BDNF and, therefore, might foster the entry of migrating cells to the stationary phase. Together, our data highlight an unexpected organization of blood vessels in the adult migratory stream and provide a func-

tional and mechanistic explanation for the long-distance saltatory migration of neuronal precursors from the posterior (SVZ) to the most anterior (OB) parts of the adult brain (for a model, see Fig. 2H).

### Blood vessels as a substrate for a long-distance migration of newborn cells in the adult brain

The mechanisms of long-distance migration of neuronal precursors in the adult brain have remained elusive. Neuronal precursors were generally assumed to course from the SVZ toward and into the OB in response to chemoattractive molecules, whereas chemorepellent cues were thought to keep these cells in the migratory stream and impede their invasion of neighboring territories. Although *in vitro* studies suggested the existence of such chemoattractive cues (Ng et al., 2005; Paratcha et al., 2006), surgical removal of the OB *in vivo* did not affect migration of neuronal precursors (Jankovski et al., 1998; Kirschenbaum et al., 1999). With regard to the chemorepellent molecules, it has been demonstrated that the septum (Wu et al., 1999) and the choroid plexus (Sawamoto et al., 2006) secrete Slit, a molecule that repels neuronal precursors from the posterior parts of the brain. The gradient of Slit is created by the beating of cilia of the ependymal cells bordering lateral ventricle (Sawamoto et al., 2006). Although this gradient is important for the navigation of migrating cells in the SVZ (Sawamoto et al., 2006), it is difficult to imagine how the unidirectional vectorial gradient of a single molecule might explain the complex-shaped curvature migration of newborn cells in the RMS. For newborn cells to remain in the RMS and migrate through various brain regions toward and into OB, all RMS-neighboring territories would have to secrete chemorepellent guidance cues. However, because the adult migratory stream has a very complex curvature architecture, gradients of many different chemorepellent molecules would be required to ensure faithful migration of newborn cells (Fig. 2H). The vasculature-guided migration hypothesis proposed here offers a much simpler and cogent explanation of the functional organization of the long-distance journey of newborn cells from caudal to the most rostral parts of the forebrain (for a model, see Fig. 2H). This hypothesis allows us to envisage the organization of the migratory pathway in the adult forebrain without a requirement for myriad chemoattractive, chemorepellent, and chemopermissive cues. In the context of newborn cells migrating along blood vessels, a single repellent molecule might be sufficient to push cells away from the posterior parts of the brain (Wu et al., 1999; Sawamoto et al., 2006), with vasculature providing local cues (BDNF and likely many others) to keep migrating precursors in the RMS and guide them in the adult forebrain. In such a perspective, the major difficulty for migrating cells is to “jump” in the core of the OB from the blood vessels oriented parallel to the tangentially migrating cells to the ones that are oriented perpendicularly and start thereafter radial migration. It seems that this is indeed a difficult task for migrating cells because many of them become lost and detached from vasculature in the core of OB. However, the cells that succeed in exiting from the RMS<sub>OB</sub> and start their radial migration do this along blood vessels. In accordance with our results are observations showing close association of radially migrating cells in the OB with blood vessels (Bovetti et al., 2007).

### BDNF and mechanisms of vasculature-associated migration of newborn cells

BDNF plays an important role in the neuronal migration during development (Polleux et al., 2002; Marín and Rubenstein, 2003;

Zhou et al., 2007). Here, by modulating the level of BDNF expression specifically in the adults, we show that vasculature-derived BDNF controls neuronal migration in the adult SVZ–OB pathway. Interestingly, the effect of BDNF is directly mediated by p75NTR present on the neuroblast. Several studies have examined the expression pattern of p75NTR in the SVZ and RMS of adult and young animals [postnatal day 7 (P7)] (Giuliani et al., 2004; Gascon et al., 2007; Young et al., 2007; Bath et al., 2008; Galvão et al., 2008). Although most of the p75NTR immunoreactivity in the adult SVZ was associated with a small fraction of proliferating nestin<sup>+</sup> cells (Giuliani et al., 2004; Young et al., 2007), some of the migrating neuronal precursors have been also shown to express p75NTR (Young et al., 2007; Galvão et al., 2008). p75NTR is not observed in the RMS of young animals (P7) (Gascon et al., 2007), but, when neuronal precursors are cultured *in vitro*, they start to express high levels of this neurotrophic receptor (Gascon et al., 2005). Recently, it has been reported that, in the adult RMS, p75NTR is present on rapidly dividing C-type cells (Bath et al., 2008). This population of cells is, however, essentially undetectable in electron microscopic studies of the adult RMS (Doetsch et al., 1997; Gritti et al., 2002). Another study that has examined expression of p75NTR in the adult RMS has reported the presence of “immunoreactive cells assembled in the continuous chains and elongated in the direction parallel to the migratory stream” (Giuliani et al., 2004), consistent with the data reported here. Using immunolabeling with cell-type-specific markers, semiquantitative RT-PCR of FACS-purified neuroblasts and astrocytes, function-blocking antibodies for p75NTR, genetically engineered mice deficient for this receptor, and time-lapse video microscopy of cell migration, we demonstrated that p75NTR is expressed by migrating neuroblasts in the adult RMS and controls their migration in response to BDNF. It has been shown previously that p75NTR is involved in axonal growth, as well as the migration of glioma and Schwann cells (Anton et al., 1994; Johnston et al., 2007). Intriguingly, 28 d after BrdU injection, no differences in the number of BrdU<sup>+</sup> cells was detected in the OB of p75NTR-deficient animals (Bath et al., 2008). These data suggest that different survival rates of newly arrived neurons in the OB of p75NTR-deficient mice compared with wild-type littermates might be involved. Together with recently published data implicating this receptor in the neuroblasts production (Young et al., 2007), our data indicate that p75NTR plays a dual role in the adult OB neurogenesis by controlling the generation of neuronal precursors (Young et al., 2007) and their migration toward and into OB.

Our data also suggest that the migrating neuroblasts themselves might regulate the level of extracellular BDNF and, therefore, the duration of their migratory phase. GABA released from migrating neuroblasts induces Ca<sup>2+</sup> fluctuations in astrocytes through activation of GABA<sub>A</sub> receptors. This Ca<sup>2+</sup> activity led to the insertion of high-affinity TrkB receptors on the plasma membrane of astrocytes and subsequently to the trapping of extracellular BDNF. We hypothesize that, through this mechanism, neuroblasts can control the periodicity of their migratory and stationary phases. Thus, the astrocytes that ensheath neuronal precursors (Alvarez-Buylla and Garcia-Verdugo, 2002; Lledo and Saghatelian, 2005) and contact blood vessels play an important regulatory role in the vasculature-associated migration of neuronal precursors, because they regulate the amount of free BDNF available to migrating neuronal precursors. Our data, therefore, reveal a novel mechanism by which astrocytes regulate neuronal migration in the adult RMS. In agreement with this are our results showing that conditional removal of TrkB receptors on as-

trocytes drastically affects neuronal migration in the adult brain. It is conceivable that neuronal precursors undergo stationary periods to accumulate energy and receive additional signals for their migration. We hypothesize that removing this important regulatory cascade that ensures periodicity of migratory and stationary phases leads to the abnormal migration of neuronal precursors and, therefore, to reduced number of BrdU<sup>+</sup> cells in the OB 5 d after BrdU injection. Our data are in line with recently reported reduction in the number of BrdU<sup>+</sup> cells, 28 d after BrdU injection, in TrkB haploinsufficient mice (Bath et al., 2008). This effect was, however, attributed to the role of TrkB receptors expressed on neuroblasts (Chiaromello et al., 2007; Bath et al., 2008). Here, using acute slices prepared from the adult forebrain, we were not able to detect any effect of TrkB inhibitor on neuronal migration. In addition, application of BDNF or TrkB–Fc in the slices prepared from p75NTR-deficient mice and direct real-time monitoring of cell migration did not reveal any differences in the migratory behavior of neuroblasts. These results are in line with the recently proposed role for TrkB receptors in the adult SVZ–RMS pathway (Galvão et al., 2008). Together, the mechanisms described here offer a simple and cogent explanation of long-range migration of neuronal precursors in the adult brain.

## References

- Alderson RF, Curtis R, Alterman AL, Lindsay RM, DiStefano PS (2000) Truncated TrkB mediates the endocytosis and release of BDNF and neurotrophin-4/5 by rat astrocytes and schwann cells *in vitro*. *Brain Res* 871:210–222.
- Altman J, Das GD (1966) Autoradiographic and histological studies of postnatal neurogenesis. I. A longitudinal investigation of the kinetics, migration and transformation of cells incorporating tritiated thymidine in neonate rats, with special reference to postnatal neurogenesis in some brain regions. *J Comp Neurol* 126:337–389.
- Alvarez-Buylla A, Garcia-Verdugo JM (2002) Neurogenesis in adult subventricular zone. *J Neurosci* 22:629–634.
- Anton ES, Weskamp G, Reichardt LF, Matthew WD (1994) Nerve growth factor and its low-affinity receptor promote Schwann cell migration. *Proc Natl Acad Sci U S A* 91:2795–2799.
- Anton ES, Ghoshghaei HT, Weber JL, McCann C, Fischer TM, Cheung ID, Gassmann M, Messing A, Klein R, Schwab MH, Lloyd KC, Lai C (2004) Receptor tyrosine kinase ErbB4 modulates neuroblast migration and placement in the adult forebrain. *Nat Neurosci* 7:1319–1328.
- Bath KG, Mandairon N, Jing D, Rajagopal R, Kapoor R, Chen ZY, Khan T, Proenca CC, Kraemer R, Cleland TA, Hempstead BL, Chao MV, Lee FS (2008) Variant brain-derived neurotrophic factor (Val66Met) alters adult olfactory bulb neurogenesis and spontaneous olfactory discrimination. *J Neurosci* 28:2383–2393.
- Bédard A, Parent A (2004) Evidence of newly generated neurons in the human olfactory bulb. *Brain Res Dev Brain Res* 151:159–168.
- Belvindrah R, Hankel S, Walker J, Patton BL, Müller U (2007) Beta1 integrins control the formation of cell chains in the adult rostral migratory stream. *J Neurosci* 27:2704–2717.
- Benraiss A, Chmielnicki E, Lerner K, Roh D, Goldman SA (2001) Adenoviral brain-derived neurotrophic factor induces both neostriatal and olfactory neuronal recruitment from endogenous progenitor cells in the adult forebrain. *J Neurosci* 21:6718–6731.
- Berthod F, Germain L, Tremblay N, Auger FA (2006) Extracellular matrix deposition by fibroblasts is necessary to promote capillary-like tube formation *in vitro*. *J Cell Physiol* 207:491–498.
- Bolteus AJ, Bordey A (2004) GABA release and uptake regulate neuronal precursor migration in the postnatal subventricular zone. *J Neurosci* 24:7623–7631.
- Bovetti S, Hsieh YC, Bovolin P, Perroteau I, Kazunori T, Puche AC (2007) Blood vessels form a scaffold for neuroblast migration in the adult olfactory bulb. *J Neurosci* 27:5976–5980.
- Chiaromello S, Dalmaso G, Bezin L, Marcel D, Jourdan F, Peretto P, Fasolo A, De Marchis S (2007) BDNF/TrkB interaction regulates migration of SVZ precursor cells via PI3-K and MAP-K signalling pathways. *Eur J Neurosci* 26:1780–1790.

- Clary DO, Reichardt LF (1994) An alternatively spliced form of the nerve growth factor receptor TrkA confers an enhanced response to neurotrophin 3. *Proc Natl Acad Sci U S A* 91:11133–11137.
- Conover JC, Doetsch F, Garcia-Verdugo JM, Gale NW, Yancopoulos GD, Alvarez-Buylla A (2000) Disruption of Eph/ephrin signaling affects migration and proliferation in the adult subventricular zone. *Nat Neurosci* 3:1091–1097.
- Cremer H, Lange R, Christoph A, Plomann M, Vopper G, Roes J, Brown R, Baldwin S, Kraemer P, Scheff S, Barthels D, Rajewsky K, Wille W (1994) Inactivation of the N-CAM gene in mice results in size reduction of the olfactory bulb and deficits in spatial learning. *Nature* 367:455–459.
- Doetsch F, Garcia-Verdugo JM, Alvarez-Buylla A (1997) Cellular composition and three-dimensional organization of the subventricular germinal zone in the adult mammalian brain. *J Neurosci* 17:5046–5061.
- Du J, Feng L, Zaitsev E, Je HS, Liu XW, Lu B (2003) Regulation of TrkB receptor tyrosine kinase and its internalization by neuronal activity and  $Ca^{2+}$  influx. *J Cell Biol* 163:385–395.
- Fraser DD, Duffy S, Angelides KJ, Perez-Velazquez JL, Kettenmann H, MacVicar BA (1995) GABA<sub>A</sub>/benzodiazepine receptors in acutely isolated hippocampal astrocytes. *J Neurosci* 15:2720–2732.
- Galvão RP, Garcia-Verdugo JM, Alvarez-Buylla A (2008) Brain-derived neurotrophic factor signaling does not stimulate subventricular zone neurogenesis in adult mice and rats. *J Neurosci* 28:13368–13383.
- Gascon E, Vutsits L, Zhang H, Barral-Moran MJ, Kiss PJ, Mas C, Kiss JZ (2005) Sequential activation of p75 and TrkB is involved in dendritic development of subventricular zone-derived neuronal progenitors in vitro. *Eur J Neurosci* 21:69–80.
- Gascon E, Vutsits L, Jenny B, Durbec P, Kiss JZ (2007) PSA-NCAM in postnatally generated immature neurons of the olfactory bulb: a crucial role in regulating p75 expression and cell survival. *Development* 134:1181–1190.
- Giuliani A, D'Intino G, Paradisi M, Giardino L, Calzà L (2004) p75(NTR)-immunoreactivity in the subventricular zone of adult male rats: expression by cycling cells. *J Mol Histol* 35:749–758.
- Goggi J, Pullar IA, Carney SL, Bradford HF (2003) The control of [125I]BDNF release from striatal rat brain slices. *Brain Res* 967:201–209.
- Gritti A, Bonfanti L, Doetsch F, Caille I, Alvarez-Buylla A, Lim DA, Galli R, Verdugo JM, Herrera DG, Vescovi AL (2002) Multipotent neural stem cells reside into the rostral extension and olfactory bulb of adult rodents. *J Neurosci* 22:437–445.
- Guo S, Kim WJ, Lok J, Lee SR, Besancon E, Luo BH, Stins MF, Wang X, Dedhar S, Lo EH (2008) Neuroprotection via matrix-trophic coupling between cerebral endothelial cells and neurons. *Proc Natl Acad Sci U S A* 105:7582–7587.
- Hack I, Bancila M, Loulier K, Carroll P, Cremer H (2002) Reelin is a detachment signal in tangential chain-migration during postnatal neurogenesis. *Nat Neurosci* 5:939–945.
- Hinds JW (1968) Autoradiographic study of histogenesis in the mouse olfactory bulb. II. Cell proliferation and migration. *J Comp Neurol* 134:305–322.
- Hu H, Tomasiewicz H, Magnuson T, Rutishauser U (1996) The role of polysialic acid in migration of olfactory bulb interneuron precursors in the subventricular zone. *Neuron* 16:735–743.
- Jankovski A, Sotelo C (1996) Subventricular zone-olfactory bulb migratory pathway in the adult mouse: cellular composition and specificity as determined by heterochronic and heterotopic transplantation. *J Comp Neurol* 371:376–396.
- Jankovski A, Garcia C, Soriano E, Sotelo C (1998) Proliferation, migration and differentiation of neuronal progenitor cells in the adult mouse subventricular zone surgically separated from its olfactory bulb. *Eur J Neurosci* 10:3853–3868.
- Johnston AL, Lun X, Rahn JJ, Liacini A, Wang L, Hamilton MG, Parney IF, Hempstead BL, Robbins SM, Forsyth PA, Senger DL (2007) The p75 neurotrophin receptor is a central regulator of glioma invasion. *PLoS Biol* 5:e212.
- Kirschenbaum B, Doetsch F, Lois C, Alvarez-Buylla A (1999) Adult subventricular zone neuronal precursors continue to proliferate and migrate in the absence of the olfactory bulb. *J Neurosci* 19:2171–2180.
- Lee KF, Li E, Huber LJ, Landis SC, Sharpe AH, Chao MV, Jaenisch R (1992) Targeted mutation of the gene encoding the low affinity NGF receptor p75 leads to deficits in the peripheral sensory nervous system. *Cell* 69:737–749.
- Leventhal C, Rafii S, Rafii D, Shahar A, Goldman SA (1999) Endothelial trophic support of neuronal production and recruitment from the adult mammalian subependyma. *Mol Cell Neurosci* 13:450–464.
- Liu X, Wang Q, Haydar TF, Bordey A (2005) Nonsynaptic GABA signaling in postnatal subventricular zone controls proliferation of GFAP-expressing progenitors. *Nat Neurosci* 8:1179–1187.
- Lledo PM, Saghatelian A (2005) Integrating new neurons into the adult olfactory bulb: joining the network, life-death decisions, and the effects of sensory experience. *Trends Neurosci* 28:248–254.
- Lois C, Garcia-Verdugo JM, Alvarez-Buylla A (1996) Chain migration of neuronal precursors. *Science* 271:978–981.
- Louissaint A Jr, Rao S, Leventhal C, Goldman SA (2002) Coordinated interaction of neurogenesis and angiogenesis in the adult songbird brain. *Neuron* 34:945–960.
- Marin O, Rubenstein JL (2003) Cell migration in the forebrain. *Annu Rev Neurosci* 26:441–483.
- Mason HA, Ito S, Corfas G (2001) Extracellular signals that regulate the tangential migration of olfactory bulb neuronal precursors: inducers, inhibitors, and repellents. *J Neurosci* 21:7654–7663.
- Minichiello L, Korte M, Wolfner D, Kühn R, Unsicker K, Cestari V, Rossi-Arnaud C, Lipp HP, Bonhoeffer T, Klein R (1999) Essential role for TrkB receptors in hippocampus-mediated learning. *Neuron* 24:401–414.
- Mori T, Tanaka K, Buffo A, Wurst W, Kühn R, Götz M (2006) Inducible gene deletion in astroglia and radial glia—a valuable tool for functional and lineage analysis. *Glia* 54:21–34.
- Murase S, Horwitz AF (2002) Deleted in colorectal carcinoma and differentially expressed integrins mediate the directional migration of neural precursors in the rostral migratory stream. *J Neurosci* 22:3568–3579.
- Ng KL, Li JD, Cheng MY, Leslie FM, Lee AG, Zhou QY (2005) Dependence of olfactory bulb neurogenesis on prokineticin 2 signaling. *Science* 308:1923–1927.
- Ono K, Tomasiewicz H, Magnuson T, Rutishauser U (1994) N-CAM mutation inhibits tangential neuronal migration and is phenocopied by enzymatic removal of polysialic acid. *Neuron* 13:595–609.
- Ono M, Yanagawa Y, Koyano K (2005) GABAergic neurons in inferior colliculus of the GAD67-GFP knock-in mouse: electrophysiological and morphological properties. *Neurosci Res* 51:475–492.
- Paratcha G, Ibáñez CF, Ledda F (2006) GDNF is a chemoattractant factor for neuronal precursor cells in the rostral migratory stream. *Mol Cell Neurosci* 31:505–514.
- Pencea V, Bingaman KD, Wiegand SJ, Luskin MB (2001) Infusion of brain-derived neurotrophic factor into the lateral ventricle of the adult rat leads to new neurons in the parenchyma of the striatum, septum, thalamus, and hypothalamus. *J Neurosci* 21:6706–6717.
- Polleux F, Whitford KL, Dijkhuizen PA, Vitalis T, Ghosh A (2002) Control of cortical interneuron migration by neurotrophins and PI3-kinase signaling. *Development* 129:3147–3160.
- Rubio N (1997) Mouse astrocytes store and deliver brain-derived neurotrophic factor using the non-catalytic gp5trkB receptor. *Eur J Neurosci* 9:1847–1853.
- Saghatelian A, de Chevigny A, Schachner M, Lledo PM (2004) Tenascin-R mediates activity-dependent recruitment of neuroblasts in the adult mouse forebrain. *Nat Neurosci* 7:347–356.
- Sawamoto K, Wichterle H, Gonzalez-Perez O, Cholfin JA, Yamada M, Spassky N, Murcia NS, Garcia-Verdugo JM, Marin O, Rubenstein JL, Tessier-Lavigne M, Okano H, Alvarez-Buylla A (2006) New neurons follow the flow of cerebrospinal fluid in the adult brain. *Science* 311:629–632.
- Wu W, Wong K, Chen J, Jiang Z, Dupuis S, Wu JY, Rao Y (1999) Directional guidance of neuronal migration in the olfactory system by the protein Slit. *Nature* 400:331–336.
- Young KM, Merson TD, Sothibundhu A, Coulson EJ, Bartlett PF (2007) p75 neurotrophin receptor expression defines a population of BDNF-responsive neurogenic precursor cells. *J Neurosci* 27:5146–5155.
- Zhou P, Porcionatto M, Pilapil M, Chen Y, Choi Y, Tolias KF, Bikoff JB, Hong EJ, Greenberg ME, Segal RA (2007) Polarized signaling endosomes coordinate BDNF-induced chemotaxis of cerebellar precursors. *Neuron* 55:53–68.

**Supplemental Figure 1 - In situ hybridization for BDNF in the adult mouse forebrain.** (A) In situ hybridization for BDNF in the adult mouse brain. Scale bar, 100  $\mu\text{m}$  (B) In situ hybridization for BDNF and immunostaining for PECAM (red) in the adult RMS showing that endothelial cells of blood vessels synthesize BDNF. Note, that BDNF mRNA is present in the endothelial cells (arrowheads), but not in other cell types of the adult RMS (asterisks). Scale bar, 10  $\mu\text{m}$ . (C) In situ hybridization for BDNF and immunostaining for PECAM (green) in the striatum showing that endothelial cells of blood vessels in this region do not synthesize BDNF. Scale bar, 20  $\mu\text{m}$ . (D,E) In situ hybridization for BDNF in the cortex (D) and hippocampus (E). Note that BDNF mRNA has neuronal pattern of expression. Scale bar, 100  $\mu\text{m}$ .

**Supplemental Figure 2 - Expression of BDNF and TrkB in the OB and striatum.** (A,B) Expression of BDNF in the adult OB. Note, high level of expression of BDNF in the RMSOB and low level of expression in the granule cell layer (GCL) where neuroblast migration ends. Scale bar, 100  $\mu\text{m}$ . (C) Expression of BDNF in the adult RMS and striatum. Note, high level of BDNF expression in the RMS and its absence in the striatum. Scale bar, 100  $\mu\text{m}$ . (D) RT-PCR analysis for BDNF in the striatum and whole brain fraction. (E) The astrocytes adjacent to the blood vessels (green) do not contain BDNF (blue) in the striatum adjacent to the migratory stream in the adult brain. Scale bar, 10  $\mu\text{m}$ . (F) Expression of TrkB receptors in the RMSOB and GCL of the OB. Note, higher level of expression of TrkB in the RMSOB as compared to the GCL. Scale bar, 50  $\mu\text{m}$ .

**Supplemental Figure 3 - BDNF induces vasculature-associated cell migration.** (A) Stereotaxic injection of NaCl (0.9%) and BDNF (100 ng) in the striatum. Note de-routed Dcx+ neuroblasts in the striatum of BDNF-injected animals. Scale bar, 100  $\mu\text{m}$ . (B) High-magnification images of the boxed area in (A), depicting examples of Dcx+ neuroblasts (red) migrating along PECAM-

labeled blood vessel (green) in the BDNF (blue) injected animal. Scale bar, 10  $\mu\text{m}$ . (C,D) Images showing Dcx+ cells in the OB of IgG-Fc and TrkB-Fc (10  $\mu\text{g}/\text{ml}$ ) infused animals. Scale bars, 100  $\mu\text{m}$ . (E) Mean immunofluorescent intensity of Dcx+ cells in the OB slices of IgG-Fc, TrkB-Fc (10  $\mu\text{g}/\text{ml}$ ) and p75NTR function blocking antibodies (90  $\mu\text{g}/\text{ml}$ ) infused animals. (F) Images illustrating caspase+ cells in the RMS. Scale bar, 10 $\mu\text{m}$ . (G,H) Quantification of caspase+ cells following incubation of slices (G) in IgG-Fc, TrkB-Fc, BDNF and p75 function-blocking antibody for 1 hour or following osmotic minipump infusions of these reagents just above horizontal limb of RMS (H).

**Supplemental Figure 4 - Decreased number of BrdU+ cells in the RMSOB of TrkBfl/fl GLAST::CreERT2 mice.** (A) Micrographs displaying TrkB (green) and GFAP (red) immunolabeling in the RMS of TrkBfl/fl GLAST::CreERT2 (TrkBfl/fl) and TrkBwildtype/wildtype GLAST::CreERT2 (TrkBwt/wt) mice 5 days after the end of tamoxifen treatment. Note, reduced labeling for TrkB in TrkBfl/fl GLAST::CreERT2 (TrkBfl/fl) mice. Scale bar, 10  $\mu\text{m}$ . (B) Micrographs showing BrdU+ cells in the RMSOB of TrkBfl/fl GLAST::CreERT2 (TrkBfl/fl) and TrkBwildtype/wildtype GLAST::CreERT2 (TrkBwt/wt) mice 5 days following BrdU injection. Scale bar, 50  $\mu\text{m}$ . (C) Density of BrdU+ cells in the RMSOB of TrkBfl/fl GLAST::CreERT2 (TrkBfl/fl) and TrkBwildtype/wildtype GLAST::CreERT2 (TrkBwt/wt).

**Supplemental Figure 5 - Co-application of BDNF and TrkB-Fc induces different effects on the cell migration depending on the BDNF concentration.** (A,B) Individual experiment demonstrating that BDNF (10 ng/ml) and TrkB-Fc (1 $\mu\text{g}/\text{ml}$ ) co-application decreases the average distance that migrating cells propagate (A) and the percentage of cells in the migratory phase at each time-point (B). (C) Summary graph illustrating the effect of BDNF and TrkB-Fc co-application. (D,E,F) Individual experiment (D,E) and summary graph (F) demonstrating that co-application of BDNF (100 ng/ml) and TrkB-Fc

(1 $\mu$ g/ml) has no effect on the average distance that migrating cells propagate (D) and the percentage of cells that are in the migratory phase at each time-point (E). (G,H,I) Individual experiment (G,H) and summary graph (I) demonstrating that co-application of BDNF (200 ng/ml) and TrkB-Fc (1 $\mu$ g/ml) increases the average distance that migrating cells propagate (G) and the percentage of cells in the migratory phase at each time-point (H).

**Supplemental Figure 6 - Application of K252a does not affect migration of neuronal precursors.** (A,B) Individual experiment demonstrating that bath application of K252a (200 nM) does not affect the average distance that migrating cells propagate (A) and the percentage of cells that migrate at each time-point (B). The time period for K252a application is shown by a black line. Each time-point represents the average value for 20-30 cells. (C) Summary graph quantifying the effect of K252a application on the average distance that migratory cells propagates, the percentage of migratory cells and the duration of the stationary period. At least 50 stacks were averaged for each slice to obtain the mean value for the changes induced by K252a. Control values were calculated by averaging 50 stacks before K252a application.

**Supplemental Figure 7 - Role of IP3-sensitive intracellular stores in the Ca<sup>2+</sup> fluctuations in astrocytes and neuroblasts migration.** (A) Blockade of Ca<sup>2+</sup> release from IP3-sensitive intracellular Ca<sup>2+</sup> stores by 2-aminoethoxydiphenyl borate (2-APB) (100  $\mu$ M) pre-application completely abolished the effect of bicuculline on the Ca<sup>2+</sup> activity in astrocytes and ablated neuroblasts migration. (B) Summary graph showing changes in the Ca<sup>2+</sup> activity in the astrocytes following pre-incubation of slices with 2-APB followed by application of bicuculline or GABA.

**Supplemental Movie 1 - Neuronal precursors are aligned along the blood**

**vessels.** The part of rostral migratory pathway was reconstructed in three dimensions from 35 z-plane confocal optical sections taken at a step of 1  $\mu\text{m}$ . A 360° rotation of the cluster is shown. Note that blood vessels (labeled in green by Dextran-FITC) parallel migratory stream of adult neuronal precursors (RMS). Most of these neuronal precursors (stained in red by BrdU injection 5 days before analysis) are positioned close to blood vessels.

**Supplemental Movie 2 - Migration of neuronal precursors in the acute slices prepared from the adult mouse forebrain.** Time-lapse videoimaging of neuronal precursors in the acute slices prepared from the adult mouse forebrain. Time is indicated in minutes in the upper left corner. Scale bar, 10  $\mu\text{m}$ .

**Supplemental Movie 3 - Neuronal precursors migrate along the blood vessels.** GFP-labeled neuronal precursors migrates along blood vessel in the acute slices of the adult mouse forebrain. Blood vessels were labeled by injection of dextran-TexasRed to the tail vein 1 hour before preparation of acute slices. GFP-expressing retrovirus was injected into the SVZ 3 days before time-lapse imaging in the RMS. Time is indicated in minutes in the upper left corner. Scale bar, 10  $\mu\text{m}$ .

**Supplemental Movie 4 - Neuronal precursors preserve their vasculature-association via leading process.** Example of two GFP-labeled neuronal precursors that migrates along blood vessel in the acute slices of the adult mouse forebrain. The first cell has straightforward migration and consistently remains close to the blood vessel with its soma. The second cell also preserves an association with the vasculature via its leading processes despite the fact that the soma of the cell moved more than 3  $\mu\text{m}$  away from the blood vessels. Blood vessels were labeled by injection of dextran-TexasRed to the tail vein 1 hour before preparation of acute slices. GFP-expressing retrovirus was injected into the SVZ 3 days before time-lapse imaging in the RMS. Time is indicated in

minutes in the upper left corner. Scale bar, 10  $\mu\text{m}$ .

**Supplemental Movie 5 - BDNF increases migration of neuronal precursors.**

Time-lapse videoimaging of GFP-labeled neuronal precursors in the RMS of acute slices of the adult mouse forebrain. GFP-expressing retrovirus was injected into the SVZ 3 days before time-lapse imaging in the RMS. GFP+ migratory cells are labeled in green during their migratory periods and in red during their stationary periods. The beginning of BDNF (10 ng/ml) application is shown in the upper left corner. Note, increased number of GFP+ cells in the migratory phase following application BDNF. Scale bar, 10  $\mu\text{m}$ .

**Supplemental Movie 6 - TrkB-Fc decreases migration of neuronal**

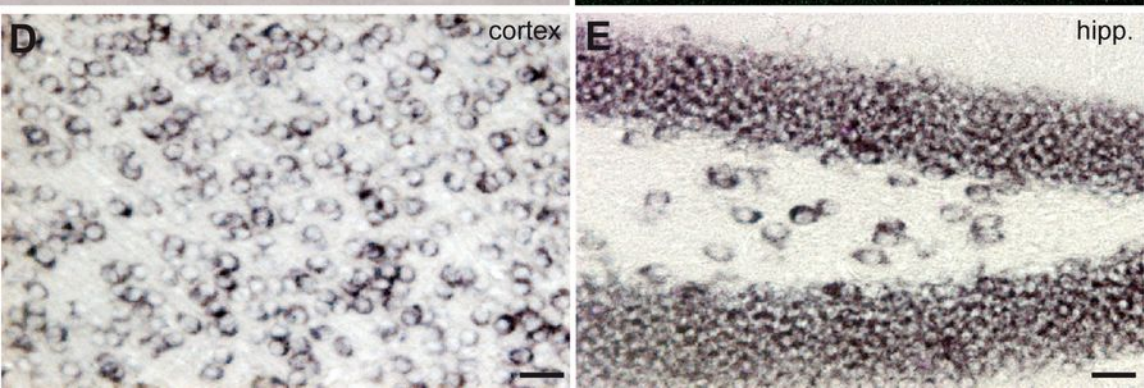
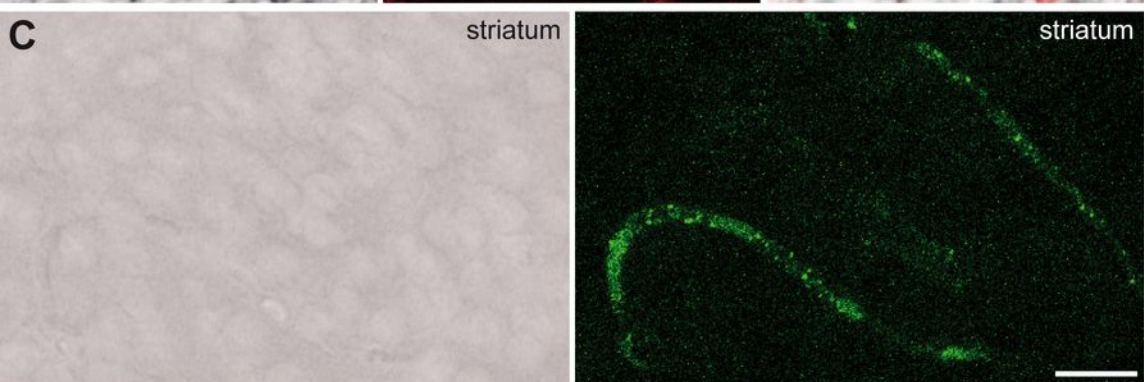
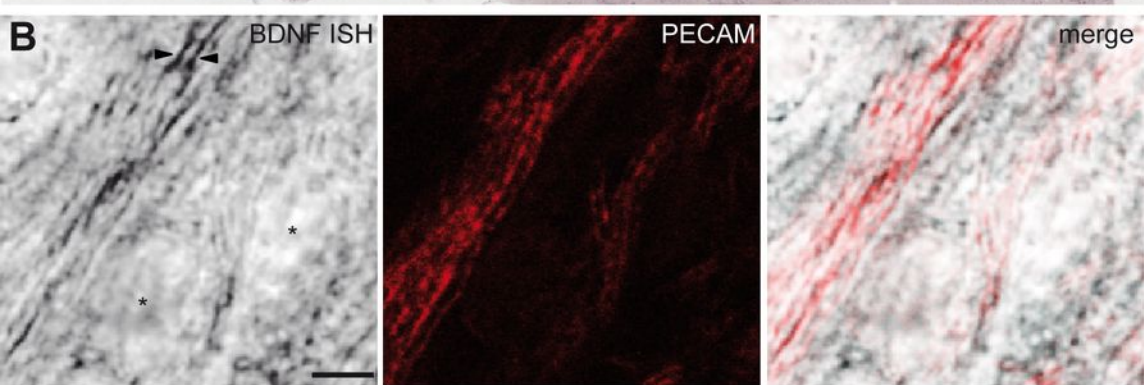
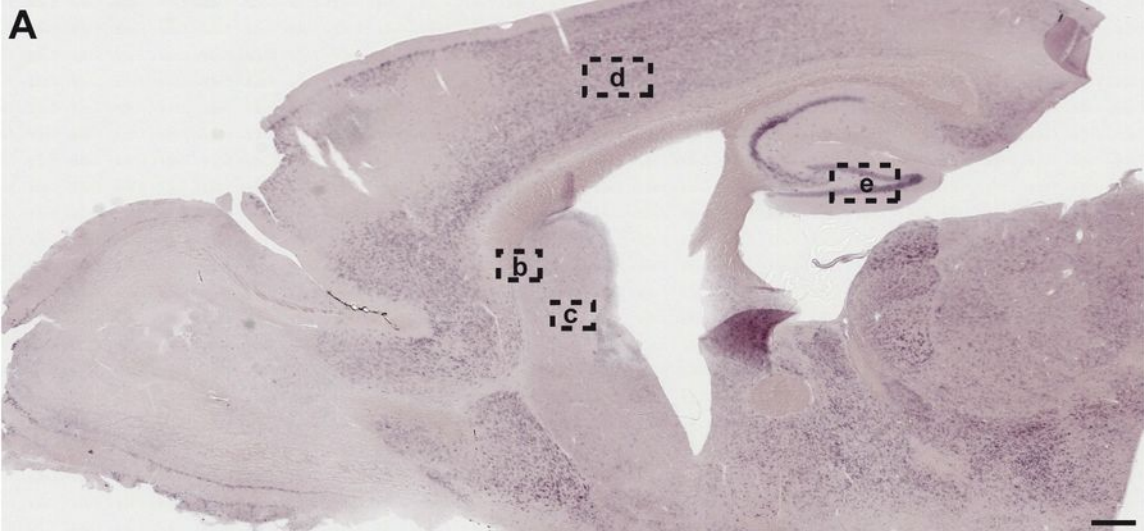
**precursors.** Time-lapse videoimaging of GFP-labeled neuronal precursors in the RMS of acute slices of the adult mouse forebrain. GFP-expressing retrovirus was injected into the SVZ 3 days before time-lapse imaging in the RMS. GFP+ migratory cells are labeled in green during their migratory periods and in red during their stationary periods. The beginning of TrkB-Fc (1  $\mu\text{g/ml}$ ) application is shown in the upper left corner. Note, decreased number of GFP+ cells in the migratory phase following TrkB-Fc application. Scale bar, 10  $\mu\text{m}$ .

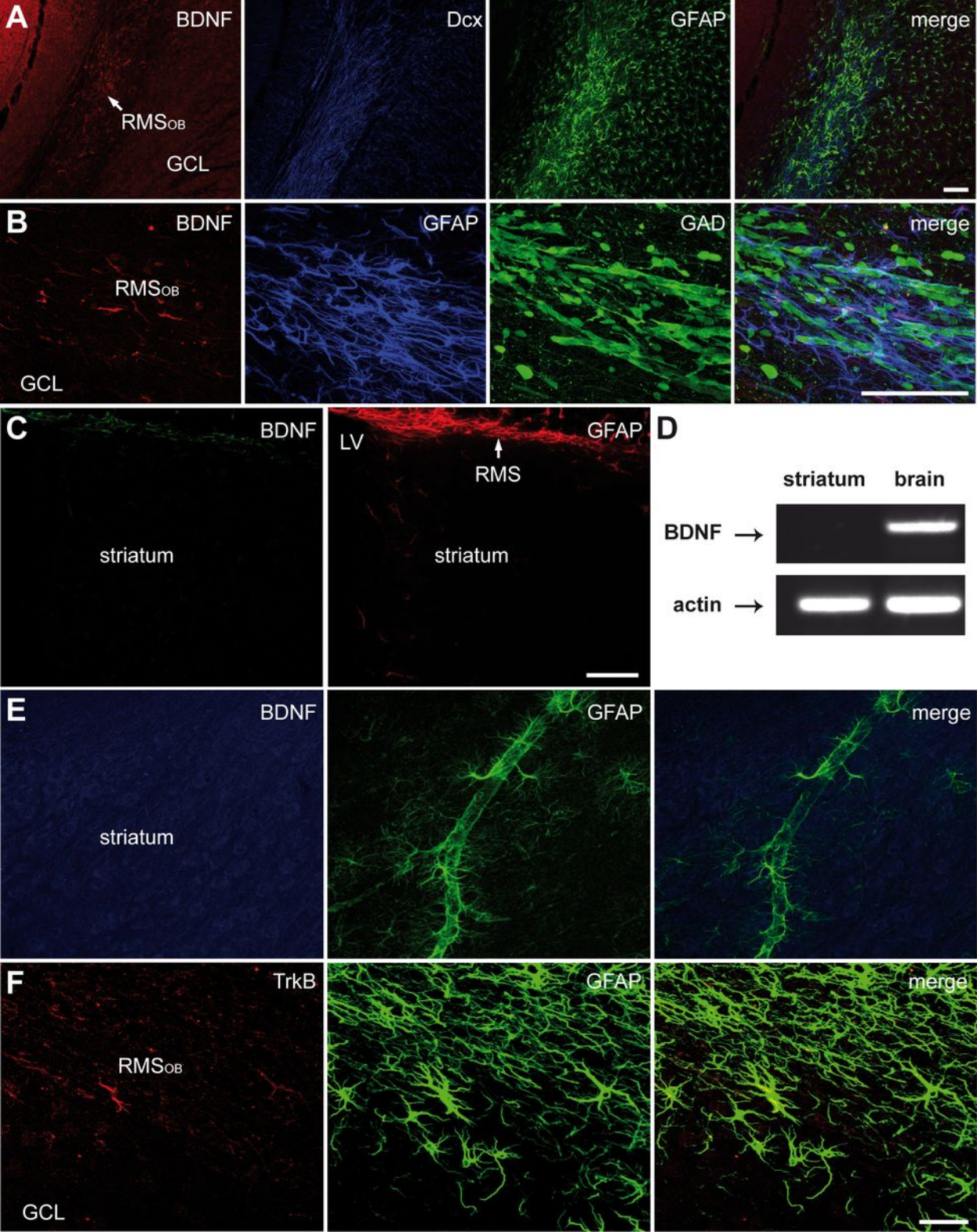
**Supplemental Movie 7 - BDNF does not affect migration of neuronal**

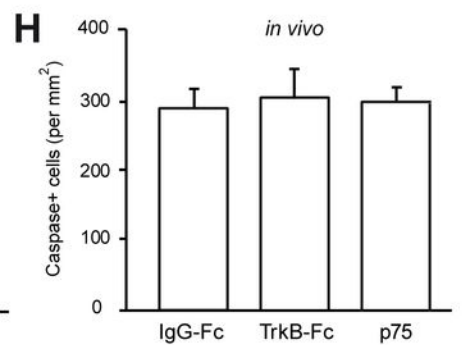
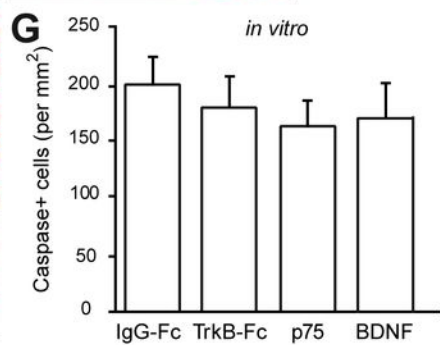
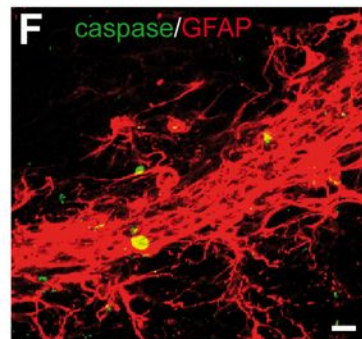
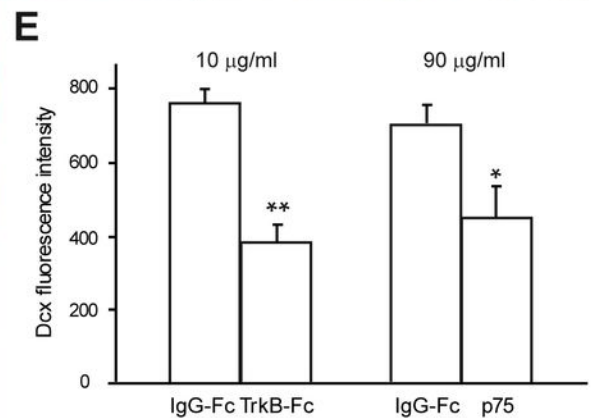
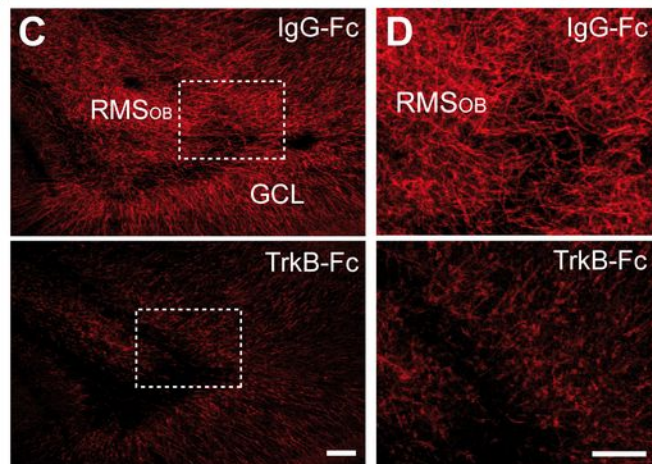
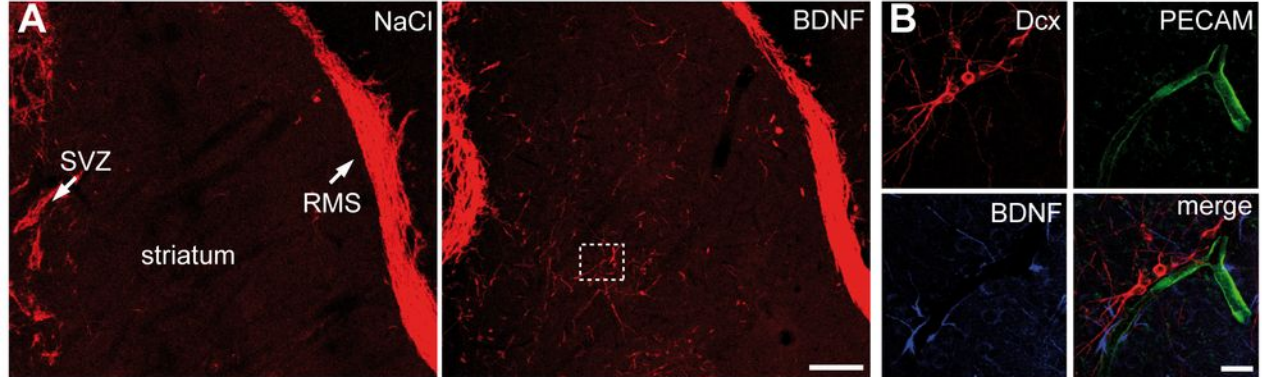
**precursors in p75NTR deficient animals.** Time-lapse videoimaging of GFP-labeled neuronal precursors in the RMS of acute slices prepared from p75NTR deficient animals. GFP-expressing retrovirus was injected into the SVZ 3 days before time-lapse imaging in the RMS. GFP+ migratory cells are labeled in green during their migratory periods and in red during their stationary periods. The beginning of BDNF (10 ng/ml) application is shown in the upper left corner. Note, reduced migration of neuronal precursors in p75NTR deficient animals and lack of BDNF effect on the neuroblasts migratory behavior. Scale bar, 10  $\mu\text{m}$ .

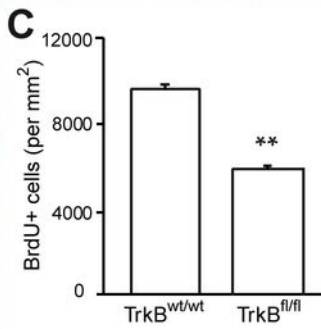
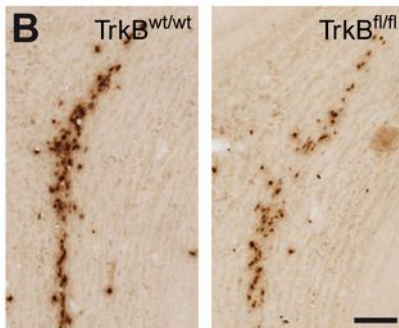
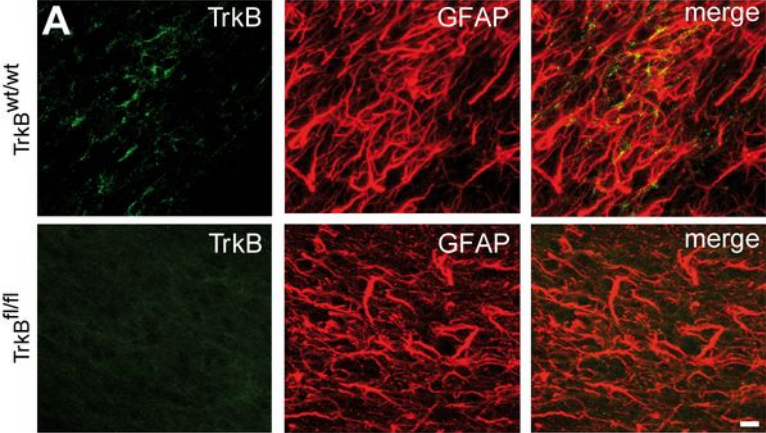
**Supplemental Movie 8 - GABA increases the frequency of Ca<sup>2+</sup> fluctuations in astrocytes.** Time-lapse videoimaging of Fluo4-labeled astrocytes in the acute slices of the RMS under control condition (left panel) and following application of GABA (10  $\mu$ M) (right panel). Note, increased Ca<sup>2+</sup> fluctuations after GABA application. Scale bar, 5  $\mu$ m.

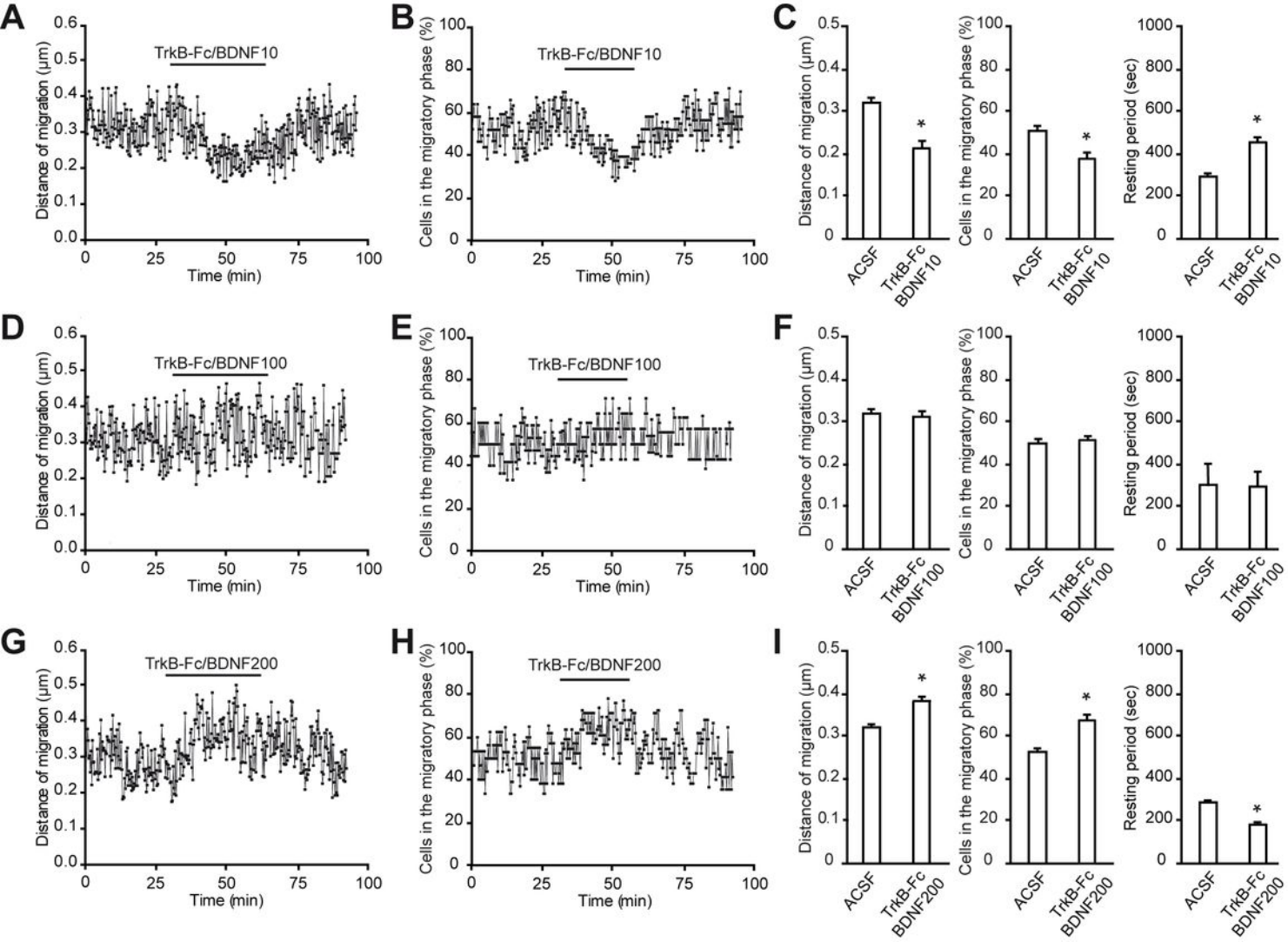
**Supplemental Movie 9 - GABAA receptor antagonist decreases the frequency of Ca<sup>2+</sup> fluctuations in astrocytes.** Time-lapse videoimaging of Fluo4-labeled astrocytes in the acute slices of the RMS under control condition (upper panel) and following application of bicuculline (100  $\mu$ M) (lower panel). Note, decreased Ca<sup>2+</sup> fluctuations after application of bicuculline. Scale bar, 10  $\mu$ m.

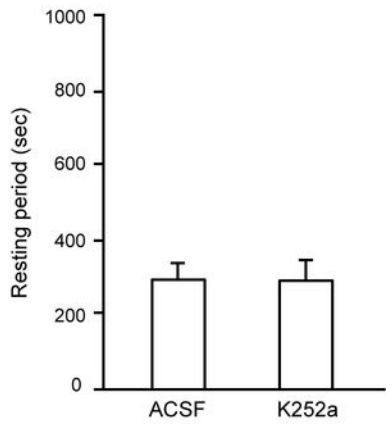
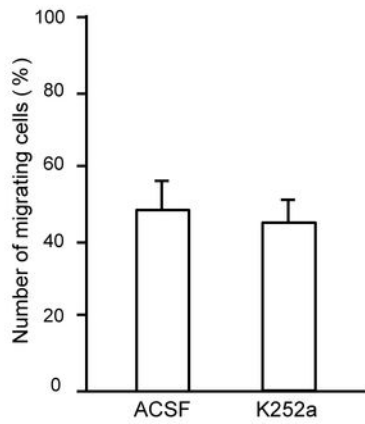
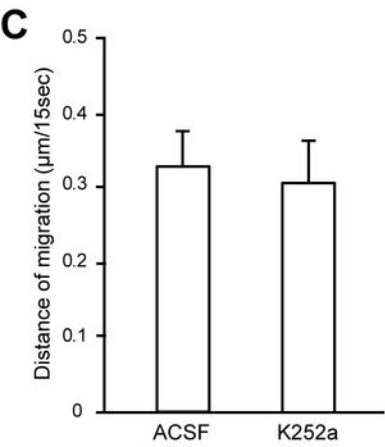
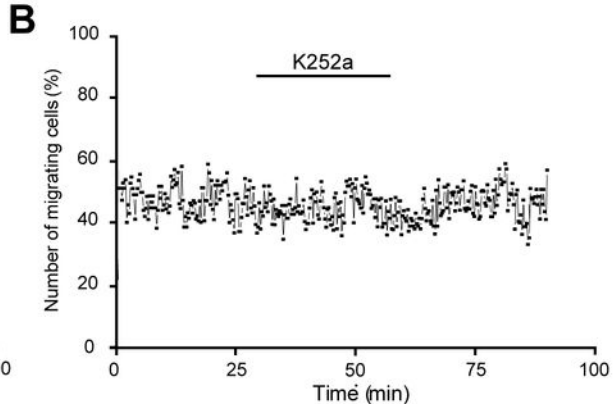
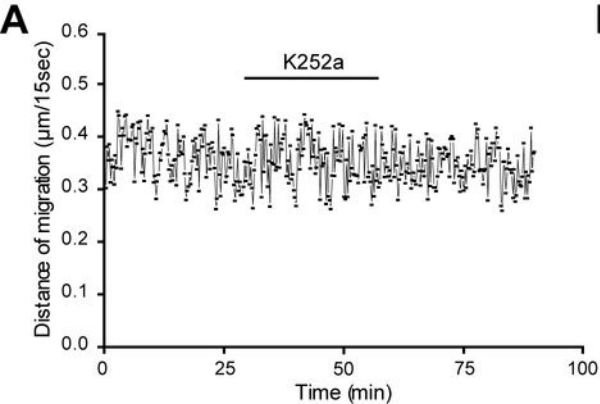


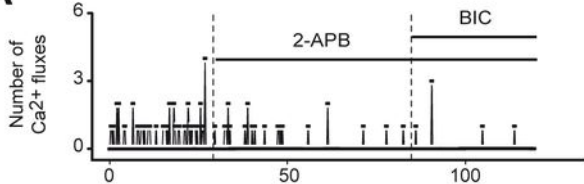










**A****B**